STARS

University of Central Florida
STARS

Retrospective Theses and Dissertations

1995

Calculating Cross Slot Flux Losses in High Voltage Stator Coils

John D. Amos
University of Central Florida, jdamos61@gmail.com

 Part of the Electrical and Computer Engineering Commons
Find similar works at: https://stars.library.ucf.edu/rtd
University of Central Florida Libraries http://library.ucf.edu

This Masters Thesis (Open Access) is brought to you for free and open access by STARS. It has been accepted for inclusion in Retrospective Theses and Dissertations by an authorized administrator of STARS. For more information, please contact STARS@ucf.edu.

STARS Citation

Amos, John D., "Calculating Cross Slot Flux Losses in High Voltage Stator Coils" (1995). *Retrospective Theses and Dissertations*. 3138.
https://stars.library.ucf.edu/rtd/3138

CALCULATING CROSS SLOT FLUX LOSSES IN HIGH VOLTAGE STATOR COILS

by

JOHN D. AMOS
BSEE, Southern University, 1989

THESIS

Submitted in partial fulfillment of the requirements
for the degree of
Master of Science in Electrical Engineering
College of Engineering
University of Central Florida
Orlando, Florida

Summer Term
1995

This thesis is dedicated to my father, John Noles Amos, Sr. in memory of the wise counsel and examples he gave that encouraged me to pursue a career in Electrical Engineering..

ACKNOWLEDGMENTS

Foremost, I would like to express my sincere appreciation to my advisor, Dr. Michael Haralambous, whose guidance and direction made this project a success. I would also like to thank Dr. Roger Johnson and Dr. Issa Batarseh for serving on my committee.

I am especially grateful to my wife, Michelle E. Amos, for the constant support and encouragement she has given me throughout my educational and professional career.

Finally, I would like to thank Mr. Calvin Paris of Westinghouse Electric for his support and advise on this project. If it were not for him this project would not have been possible.

TABLE OF CONTENTS

LIST OF TABLES

LIST OF FIGURES

INTRODUCTION

The maximum capability of an electric generator is limited primarily by the heating of its components. Temperatures developed in various parts of the generator must be within limits that will provide safe and reliable operation during its design life. In most generator components it is the highest, rather than the average temperature, that must meet the required limits.

In the United States, generators are designed based on meeting requirements or limits stated in the American National Standards Institute (ANSI). In reference to stator coils for large synchronous generators, ANSI C50.13 states that the hottest-spot temperature shall not exceed 130° C for class B insulation systems. It also states that these hottest-spot temperatures for armature windings shall be demonstrable by direct measurement or recognized methods of calculation correlated to special factory tests on a basically similar machine [1].

This means that either we have a proved method of calculating the hottest-spot temperatures that is verified with test data on a similar type machine or that we must test every machine built. Well, a complete Engineering factory test on one single large electric generator could cost in excess of one million dollars (depending on customer requests). Therefore it is very important that we continue to develop methods of

calculating losses and temperatures for all new designs which differ in design from previously tested machines.

As the cost to produce electric power increases throughout the world, the need for more efficient machines become higher in demand by the power utilities. It is, therefore, important to have uniform temperature distribution for economical and efficient utilization of all generator components, stator windings in particular.

The various types of eddy current losses taking place in the stator winding would cause non-uniform temperature distribution and utilization of the coil material, if measures to reduce them were not taken. The eddy current losses in stator coils are reduced by building the conductors of a large number of mutually insulated cooper strands which are short circuited at least at the ends of the phase group. The currents circulating between these strands are suppressed by transposing them in such ways that all strands have the same voltage induced in them. Building coils with ideal transposition patterns such that voltage balance is achieved within each individual coil side is the topic for much on-going research and development.

Because of cost and efficiency it is necessary to analyze the possibilities of using different coil constructions from those presently in use. This thesis will limit the scope to hydrogen inner-cooled stator windings for large AC electric synchronous generators. Past practice has been to use 360° roebel transpositions and therefore this is where the emphasis of past eddy loss analysis was conducted [2].

Various roebel transpositions now being introduced into stator winding designs bring new challenges to the eddy loss theory and calculation. Using past loss

calculation methods on these new coil designs tend to calculate temperatures with hot spots 15 to 20% different than test data. This large error in calculation greatly reduces the ability to achieve the full capability of new machines. Therefore, the primary purpose of this thesis is to focus on the analysis and calculation of the cross-slot eddy losses associated with these new multi-roebel transposition schemes to more accurately calculate their associated hot spot temperatures.

The eddy losses as calculated by this thesis together with the other standard stator coil losses (I^2R, radial flux losses) are used to calculate stator coil hottest-spot temperatures of the first, recently built, generator using a 720° roebel scheme with solid end connections. These calculated temperatures are compared to factory test data of this machine to validate the eddy loss calculation developed in this thesis.

Chapter 1 will provide a review of the fundamental concepts of generating electric power, explain basic stator coil construction, and briefly describe the various types of stator coil losses.

Chapter 2 will develop an improved method of calculating the cross slot flux in the slot region and its associated internal strand losses.

Chapter 3 will develop a method of calculating the strand to strand currents produced by the deep bar effect using the cross slot flux developed in chapter 2.

Chapter 4 will briefly explain the main features of the computer programs used to make the loss calculations developed in this thesis.

Chapter 5 will compare the calculated results using the above methods with test data on a production machine with the same stator coil designs described in this thesis.

I. FUNDAMENTAL CONCEPTS

GENERATING ELECTRIC POWER

In our elementary model of the steam power plant, Figure 1, we discover that a generator consists of a "bar magnet spinning inside a stationary coil of wire" which generates an electric current in the coil "as the magnetic field issuing from the ends of the magnet moves across the turns of wire in the stationary coil."

Appropriately, the stationary coil of wire is termed the stator, and the rotating magnet is termed the rotor. The rotor, however, is an electromagnet rather than a bar-magnet and is , of course, the source of magnetic lines of force. The stator is an assembly of conductors in which a voltage is induced through the relative motion of the magnetic field. In principle, it is immaterial whether the magnetic field is stationary and the conductors moving, or vice versa; however, for large turbine generators where the AC output may be as great as 300 times the DC input it is more feasible to have the magnetic field rotate and the conductors stationary. The magnetic field, or rotor, is often also referred to simply as the field, and stator as the armature or core.

Upon examination of the turbine generator, Figure 2, we see that the rotor is supported inside the stator windings on journal bearings mounted near the ends of the machine. An air gap as great as six inches exits between the rotor and stator. The

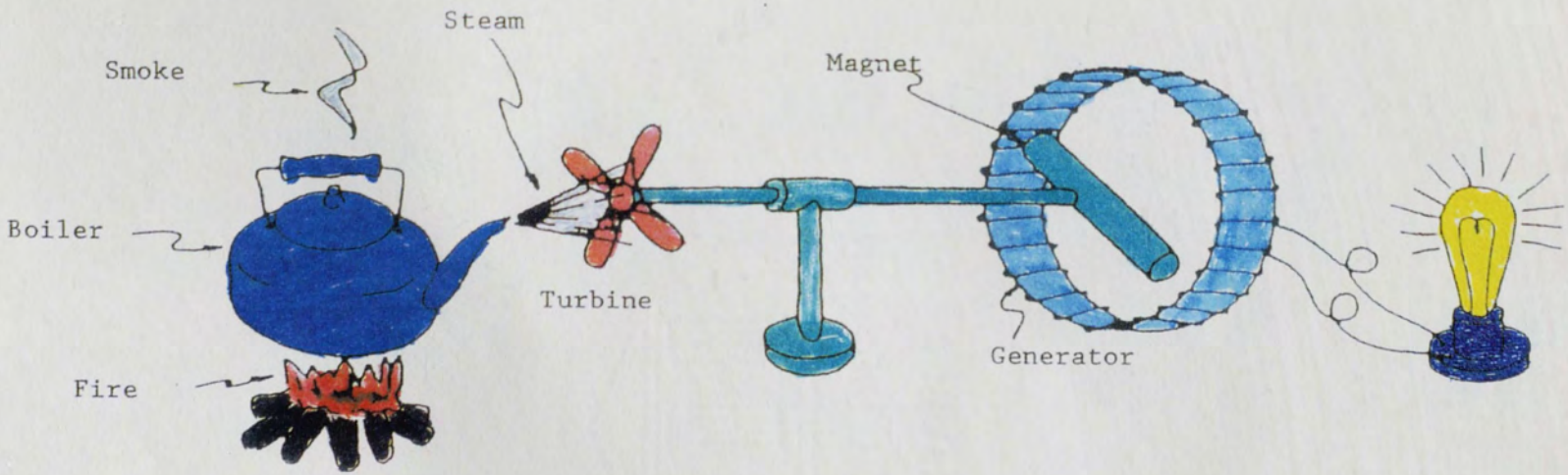

FIGURE 1. Simple Representation of Boiler, Turbine, and Generator

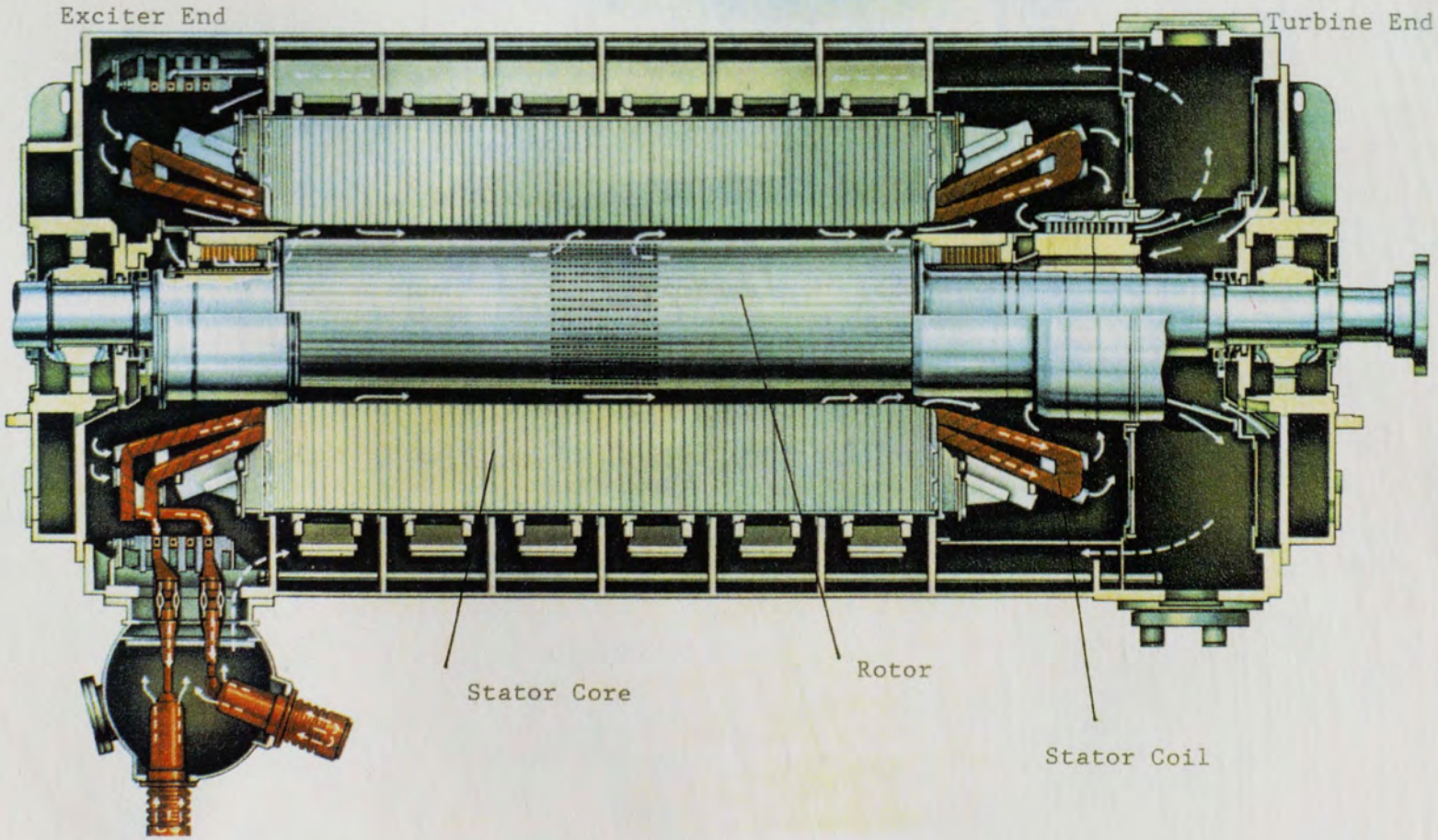

FIGURE 2. 3600-RPM Inner-Cooled Generator

mechanical energy delivered by the turbine is transferred across this air gap and appears as electrical power at the stator leads. To explain this phenomenon we observe that the rotor consists of a large steel forging with machined longitudinal slots inset with interconnected copper bars wound in such a way as to form what basically are oblong "coils" oriented about the unslotted portion of the rotor. Direct current is supplied to the coils thereby producing the magnetic field. This direct current is referred to as field current or excitation and is produced by an exciter. The direct current flows through the copper field windings of the rotor forming an even number of powerful magnetic poles in the unslotted rotor portion (Figure 3). Domestically two different rotational speeds (with the appropriate number of poles) are dictated by the necessity to produce 60 hertz (3600 RPM) for United States and 50 hertz (3000 RPM) for overseas. The magnetic flux that emerges from the "north pole of the rotor must return to the rotor through the "south pole", however this flux acts similar to water or electric current in that it takes the path of least resistance and may be guided and made to follow predetermined paths. Air exerts a high resistance (reluctance) to this flow, while iron or steel has much lower resistance. Generator design is such that the flux leaves the north pole of the rotor, crosses the air gap into the stator, goes through the stator iron and back across the air gap into the south pole, thereby completing the magnetic circuit (Figure 3). As the flux sweeps across the stator iron due to the rotor's movement, voltage is induced in copper coils mounted in the iron. This is the source of electrical power generated by the generator.

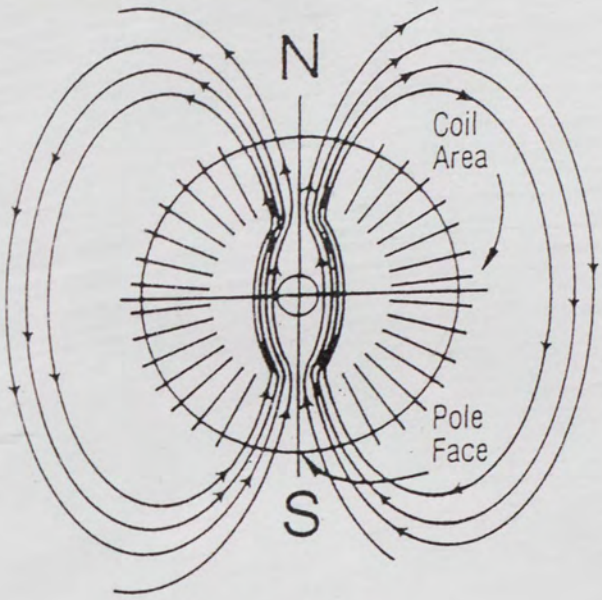

Two Pole

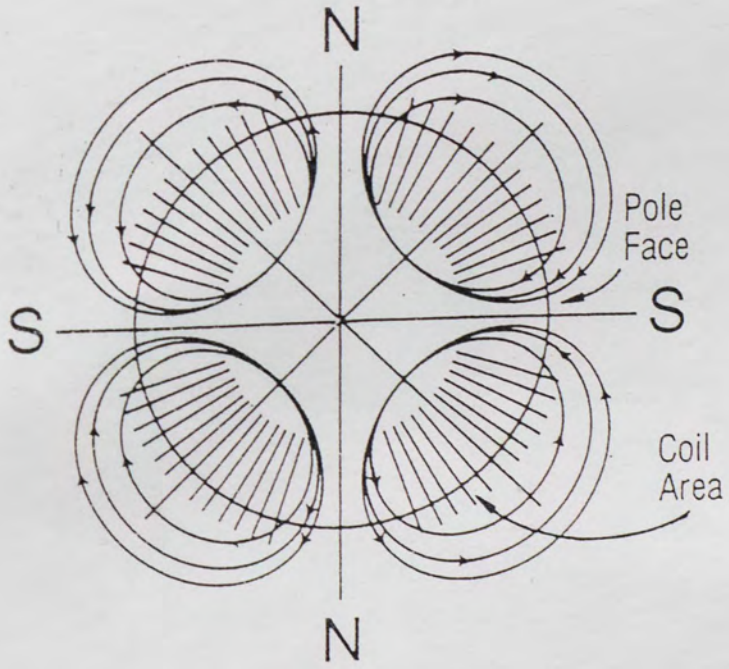

Four Pole

FIGURE 3. Flux Diagrams

The current that is produced is dependent on various parameters, including flux density, coil proportions and sweep velocity of the flux lines ($E = Blv$, a variation of the Lorentz force equation, where E being voltage generated in a conductor length "l" passing through a magnetic field of flux density B at a velocity v. The flux density, voltage, and velocity will all be at right angles to each other, the Lorentz equation being a vector relationship) [3].

After the rotating speed has been determined a rotor's primary performance characteristic curve is determined and therefore the number of lines of magnetic flux generated by the field. The desired magnetic fields can be engineered by varying the number of machined rotor slots, the number of copper bars in each slot, excitation current, and permeability (magnetic conductivity) of the rotor forging, and the length and diameter of the rotor body. The stator's design similarly can be varied around the number and depth of coil-housing stator slots parallel to the shaft, the characteristics and size of the stator iron core, coil ventilation method chosen, winding pattern of slot coils, core length, and inner and outer core diameter.

STATOR COIL CONSTRUCTION

The scope of this thesis is limited to hydrogen inner-cooled stator windings as shown in Figure 4. A typical large hydrogen cooled generator have two coils per stator slot as shown in Figure 4. The coil closer to the air gap is referred to as the top coil and the other coil is referred to as the bottom coil. A typical stator coil have several rows or

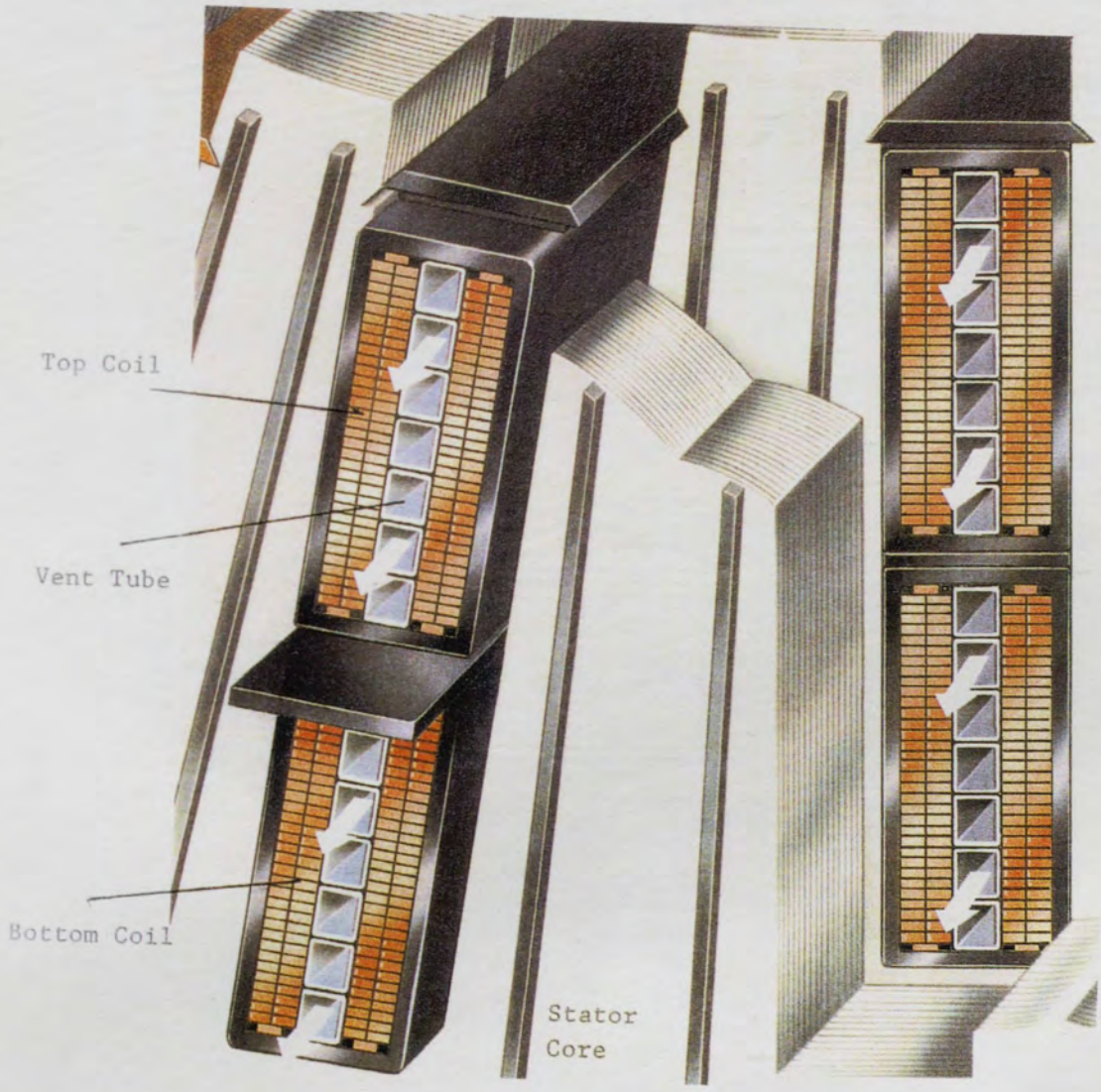

FIGURE 4. Hydrogen Inner-Cooled Stator Coils

stacks of individually insulatedstrands with a stack of vent tubes usually found in the middle of the strand stacks. The coils shown in figure 4 are referred to as a single tube stack, because they have only one stack of vent tubes. These coils are ventilated by hydrogen which passes through the vent tubes the length of the coil removing heat from the copper strands. The stator coils are secured within the stator slot by wedges which are driven in groves above the top coil.

Two strand stacks are on each side of the vent tube stack found in Figure 4. The two strand stacks located next to each other are roebelled together and called a roebel bar. Therefore the coils in Figure 4 have two roebel bars. The two roebel bars are separated by the vent tube stack in the middle. Roebelling is basically the same as taking two stacks of strands and twisting the opposite ends as if ringing the water out of a large bath towel. If you do a complete 360° twist the top right strand on one end will end up as the top right strand on the opposite end and like wise for all the other strands (Figure 5). This is referred to as a 360° roebel, and if you twist the stacks together two complete 360° you will have a 720° roebel.

To completely manufacture a stator coil, the two roebel bars with the vent tube stack in the middle are insulated with a high voltage insulation material generally called groundwall. The insulation material is grouped into classes based on the maximum temperatures it can safely be exposed to throughout the design life of the machine (previously, it was mentioned that ANSI requires that Class B insulation be exposed to less than 130° hottest-spot) [4].

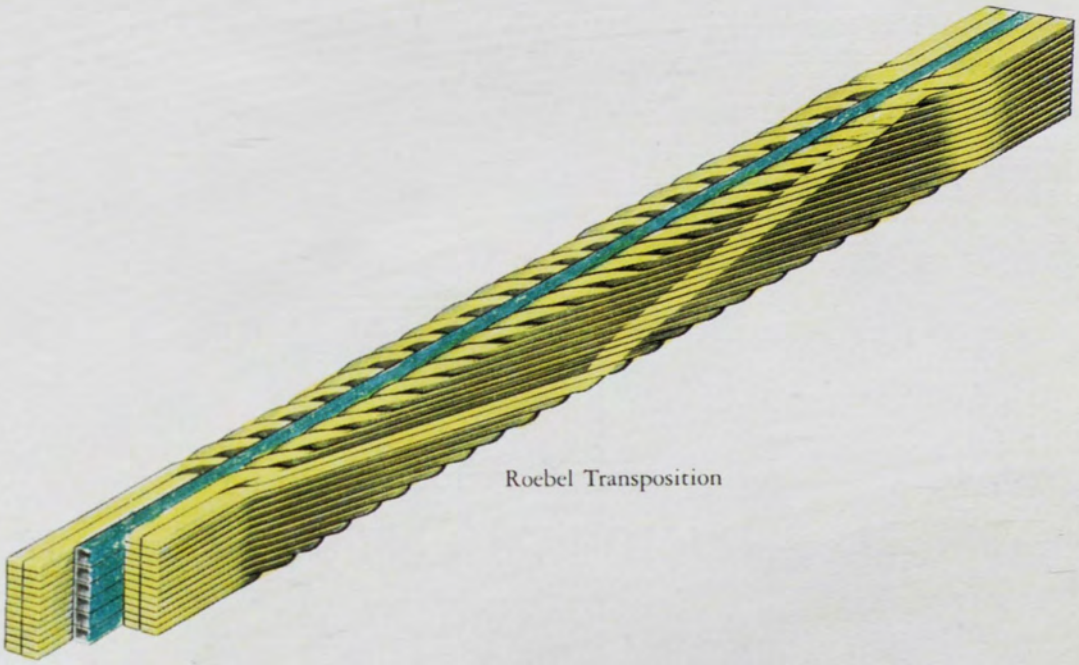

FIGURE 5. Roebel Transpositions

STATOR COIL LOSSES

The stator coils have two primary functions in a turbine generator. The generator voltage is induced in the stator winding and it conducts the load current. Performing these functions causes secondary phenomena to take place in the conductors of the stator winding. Due to the finite physical size of the conductors the same flux that links the turns of the winding links small loops inside the conductors themselves causing currents to circulate in them and generate loses [5]. The load current causes losses in the conductor's resistance. That same current excites leakage fluxes that link contours inside the conductors causing non-uniform current distribution and additional losses.

The largest loss in the stator winding is the loss due to the generator load current flowing through conductors with finite resistance. This loss has the same value as if the load current was DC and had the intensity equal to the RMS value of the AC current (I_{rms}^2R). The current in the stator winding, being located in the slots, excites a tangential flux flowing from one side wall of the slot to the other. This flux induces voltages both in the loops located inside the individual strands and in the loops formed by different strands. The radial flux that fringes from the air gap into the stator slots induces voltages in the strands and between the strands.

The losses caused by eddy currents induced inside individual strands are called eddy current losses. They are caused both by fluxes oriented tangentially and by fluxes oriented radially. The former ones are called cross slot flux eddy current losses and the latter radial flux losses. They occur both in the slot and in the end regions, with the

II. CROSS SLOT INTERNAL STRAND LOSSES

The internal strand loss within an individual strand is primarily caused by the cross slot flux in the slot region of the stator coil. Some stator slots have top and bottom coils with the same phase currents and other slots have top and bottom coils with different phase currents. The ultimate goal is to determine the highest hot spots in the coil side. Therefore, the following analysis was completed for the cross slot flux and its associated losses for each strand in a roebel bar with top and bottom coils having the same phase currents and also those slots with top and bottom coils having different phase currents.

The typical method of calculating cross slot flux is to use the average cross slot flux B_s [5]. However, it is the intent of this thesis to develop the cross slot flux and its associated losses for each individual strand in the coil side to more accurately account for the cross slot internal strand losses. The cross slot eddy loss in the top coil depends on the phase of the bottom coil in the same slot. If the coils are of the same phase the cross slot eddy loss will be higher than when the two coils are of different phases as shown later in this chapter. The basic equation for calculating cross slot eddy loss as described by William Timbie [6] states:

$$w_d = -\frac{\pi^2 f^2 B^2 T^2}{6 \cdot p \cdot 10^{16}}$$

where,

w_d = loss (watts/cubic inch)

f = frequency (hertz)

B = Flux Density (lines/in^2)

T = Thickness of conductor (in.)

p = Resistivity of material (ohm-inches)

The peak fundamental Amp-turns (MMF) for a slot with one bottom coil and one top coil (both with same phase current) is shown in Figure 6. Starting from the bottom of the slot, the Amp-turns increases for each individual strand as described by L. T. Rosenberg [7,8]. The peak MMF for one coil is determined by the following equation.

$$MMF = \sqrt{2} \cdot I_A$$

where,

MMF = Amp Turns

I_A = Phase current through coil

Likewise, the peak fundamental flux density is shown in Figure 7. The equation for determining the flux density of one coil is:

$$B = \sqrt{2} \cdot u \frac{I_A}{B_S}$$

where,

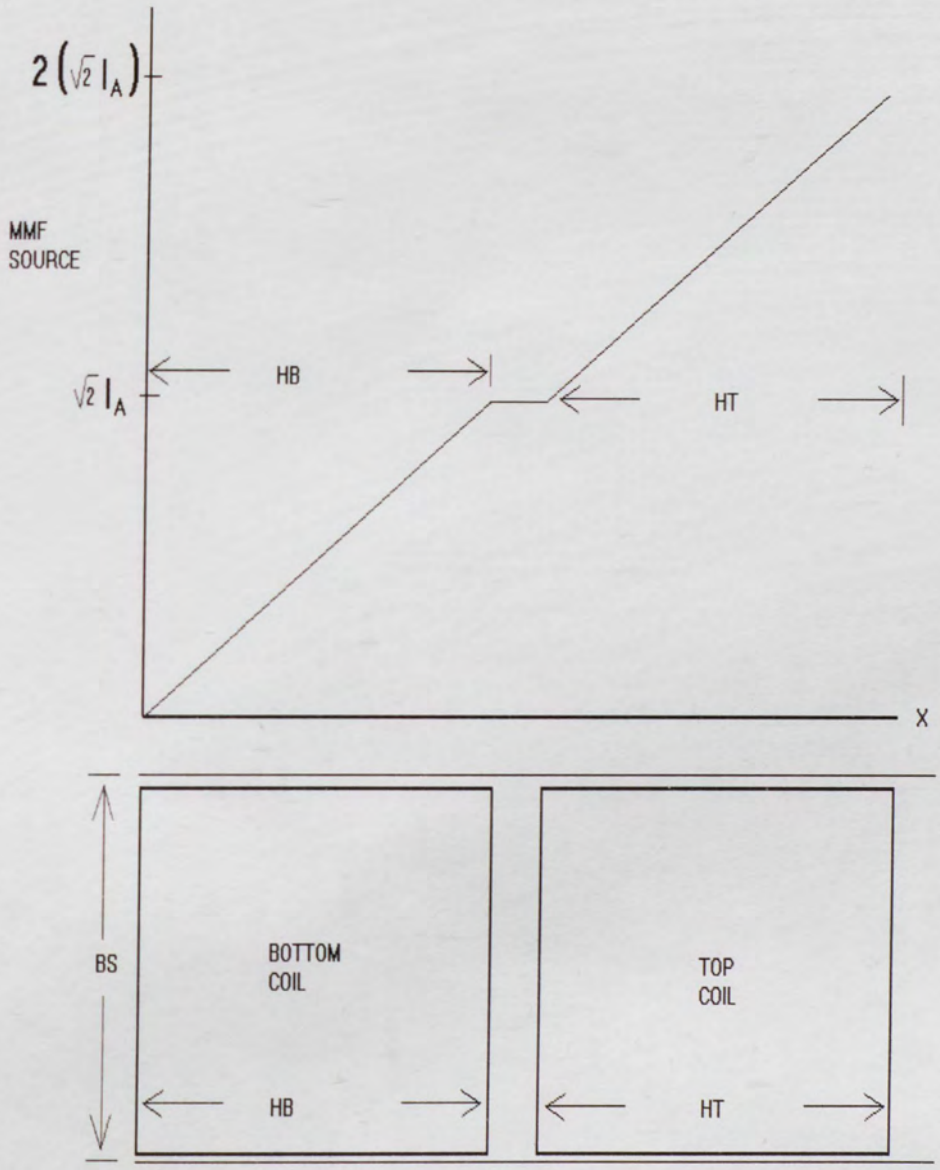

FIGURE 6. Peak Fundamental Amp-Turn/Pole
(Assumes top and bottom coil currents are in phase)

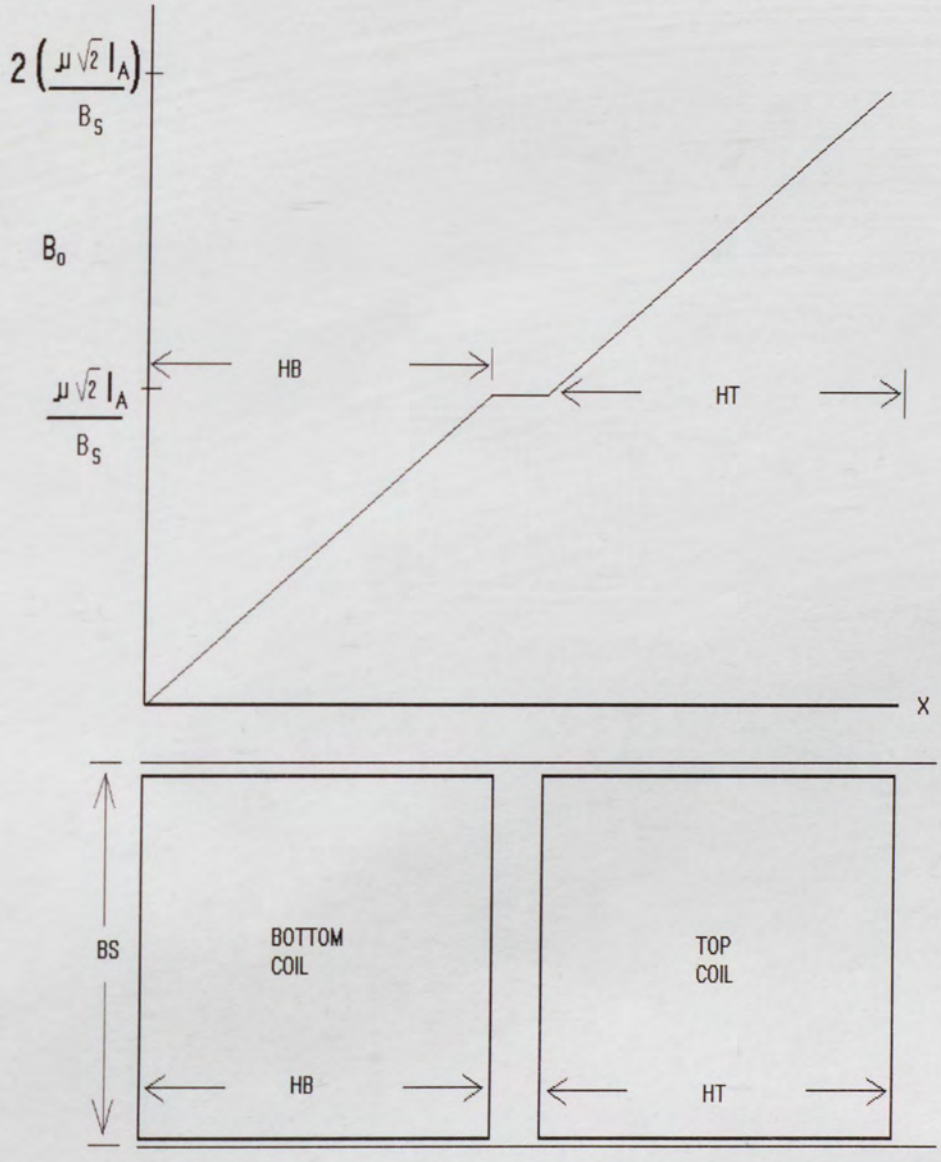

FIGURE 7. Peak Fundamental Armature Leakage Flux Density
(Assumes top and bottom coil currents are in phase)

B = Flux density

u = permeability

I_A = RMS phase current

B_S = Slot width

As shown in Figure 8 the cross slot flux density in the top coil is greater when the bottom coil is of the same phase. (The cross slot flux density of the bottom coil is not affected by the phase of the top coil. Therefore, the cross slot eddy loss is identical in all bottom coils.) When the cross slot flux density of the top coil is higher, the loss in the top coil will be higher. Since the cross slot eddy loss varies with the square of the flux density, the loss will vary with the integral of the square of the flux density. For slots where the top and bottom coils are the same ($I_{BOTT}=I_{TOP}$), the cross slot flux density will equal B_{same} as seen in Figure 8.

$$B_{same} = B_o \cdot \left(1 + \frac{x}{H_C}\right)$$

where,

$$B_o = \mu \cdot \frac{I_A}{B_S}$$

x = height from bottom of slot.

H_C = height of top coil.

For slots where the top and bottom coils are different phases, the cross slot flux density equals B_{diff} as seen in Figure 8.

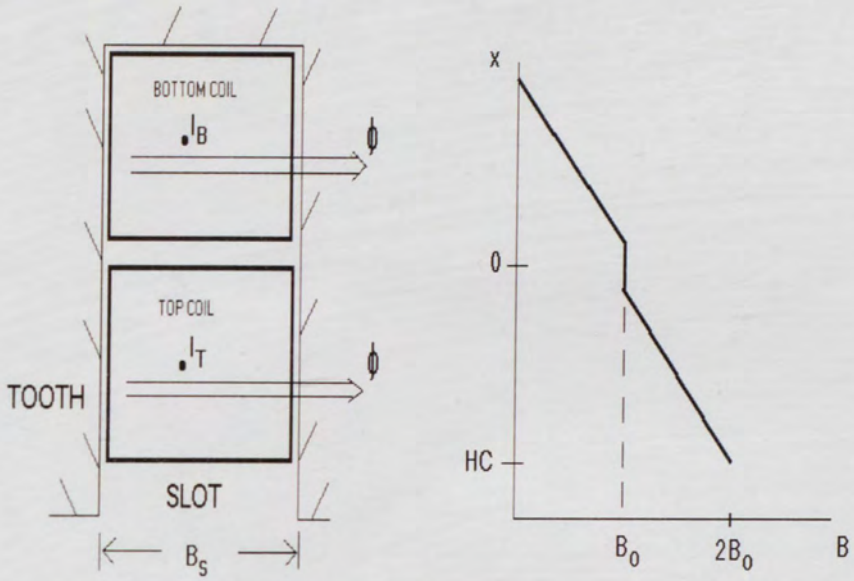

CASE 1. Top and bottom coils have same phase currents.

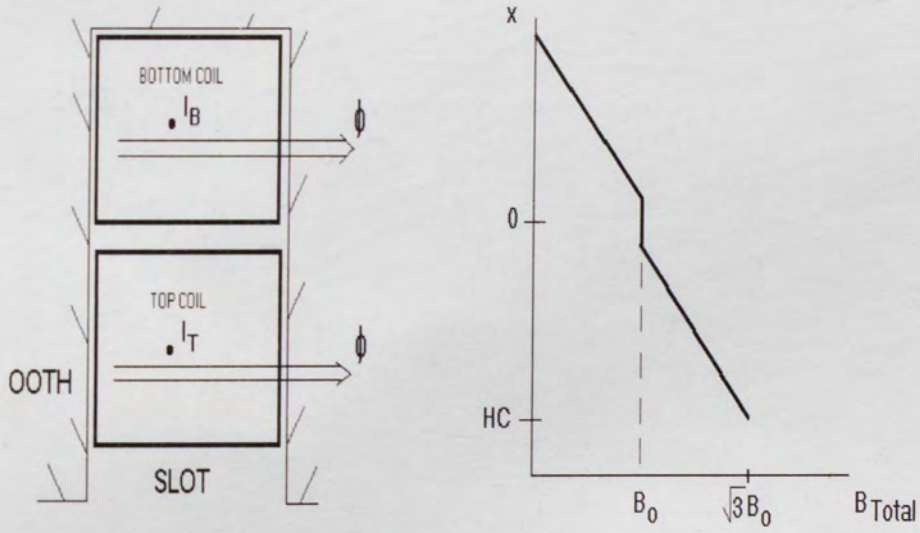

CASE 2. Top and bottom coils have different phase currents.

FIGURE 8. Flux Field Causing Cross Slot Flux

$$B_{diff} = B_o\sqrt{\left(\sqrt{3}/2\right)^2 + \left(.5 + x/H_C\right)^2}$$

where,

$I_{TOP} = I_{BOTT}$

$I_{TOP} = I_A\angle 0°$

$I_{BOTT} = (.5 + j\frac{\sqrt{3}}{2}) \cdot I_{TOP}$

$B_{TOTAL} = \sqrt{B_{REAL}{}^2 + B_{IMAJINARY}{}^2}$

$B_{REAL} = B_o \cdot (.5 + \frac{x}{H_C})$

$B_{IMAJINARY} = B_o \cdot \frac{\sqrt{3}}{2}$

Let *RLC* be the ratio of the cross slot eddy when the coils are of different phases to the cross slot eddy loss when the coils are of the same phase. Then

$$RCL = \frac{\int_0^{H_C} B_{diff}{}^2 dx}{\int_0^{H_C} B_{same}{}^2 dx} = \frac{H_C \cdot 11/6}{H_C \cdot 7/3} = 11/14$$

However this ratio of 11/4 is exact only when the number of strands is very large. With a slightly different approach we can obtain a more accurate figure. Assume that the top coil has "*n*" strands per roebel stack. Each strand will be of thickness *T*. Label the bottom strand of the top coil as strand 1 and top strand as strand "*n*". Then the cross slot flux density in the i^{th} strand will be

$$B_{same}(i) = B_o\left(1 + \frac{i}{n}\right) \qquad (1)$$

$$B_{diff}(i) = B_o\sqrt{\left(\sqrt{3}/2\right)^2 + \left(.5 + \frac{i}{n}\right)}$$

The associated cross slot flux losses are

$$w_{same} = \frac{\pi^2 f^2 T^2}{6 \cdot \rho \cdot 10^{16}} \cdot \sum_{i=1}^{n} B_{same}(i)^2 \qquad (2)$$

$$w_{diff} = \frac{\pi^2 f^2 T^2}{6 \cdot \rho \cdot 10^{16}} \cdot \sum_{i=1}^{n} B_{diff}(i)^2$$

$$RCL(n) = \frac{\sum_{i=1}^{n}\left(1 + i/n + i^2/n^2\right)}{\sum_{i=1}^{n}\left(1 + 2i/n + i^2/n^2\right)}$$

$$RCL(n) = \frac{11 \cdot n^2 + 6n + 1}{14 \cdot n^2 + 9n + 1}$$

As n approaches infinity *RCL(n)* approaches 11/14, so this derivation agrees with the first. If n equals 10 then *RCL(n)* equals 1161/1491 = .779. In decimal form 11/14 equals .0786. The disagreement between these two numbers is less that nine tenths of one percent. Note that a typical inner cooled stator coil for a large generator will have between 25 and 46 strands per stack, so the difference will be negligible.

It is shown that the worst case or largest losses will occur in slots with top and bottom coils having the same phase current. Therefore, the loss calculation in this thesis will use losses for slots with top and bottom coils having the same phase currents (equations 1 and 2) to insure calculation of the true hot spots throughout the stator coil.

III. CROSS-SLOT STRAND TO STRAND LOSSES

In turbo-generators, strands in a stator coil side are transposed to suppress additional eddy currents loss produced by alternating flux due to currents in the coil itself and in other coils. The eddy current flows in a strand from one coil end to another end, and returns through another strand because these strands are short-circuited at both ends. Generally, a bigger coil has higher eddy current loss. This effect is usually called "Deep Bar Effect".

Recently, a project was started to examine various types of transpositions and to determine cheaper coil structures. Gas inner cooled stator coils have a large cross section which results in higher deep bar effect and have less cooling effect compared with water cooled stator coils. Non-uniform current distribution by the higher deep bar effect may severely affect the hottest temperature in the gas inner cooled stator coils.

Up to this time, the deep bar effect was calculated by a computer program that only accounted for up to 360° roebels. A more flexible and accurate calculation procedure had to be developed for new coil designs. In the old program, reactance calculations were completed using a MVP (Magnetic Vector Potential) grid model [9,10,11].

In this analysis, a different approach was taken. Two separate calculations are completed. One for the slot region and one for the end regions. Reactances in the slot region are calculated by the area above strands, and it assumes that the cross slot flux goes straight across the slot. Reactances in the stator coil end regions are calculated by assuming that the flux density normal to coil side varies in proportion to the coil height. These calculations will be discussed later.

DESCRIPTION OF TRANSPOSITION MODEL AND ASSUMPTIONS

There are many coil structures and strand transpositions. Figure 9a shows some examples of these. Solid strand structures are used for conventional cooled coils and gas inner cooled coils. Hollow strand structures and composite structure of hollow and solid strands are used for water cooled coils. This thesis focuses on gas inner-cooled coil structures and its associated transpositions in the slot region and coil end region.

The strands can be transposed in various ways, one at a time or two at a time. Figure 9b shows these two cases. Direction of the transposition rotation can be clockwise or counter-clockwise (Figure 9c). In this paper, direction of rotation is defined as the view from the exciter end of the stator coil.

In this calculation, all strands in one roebel bar are numbered in the clockwise direction from 1 at the top strand in the right hand stack to n at the top strand in the left hand stack. n is the number of strands in one roebel bar. The coil is always viewed from the exciter end. With the advancement along the coil all strands change their

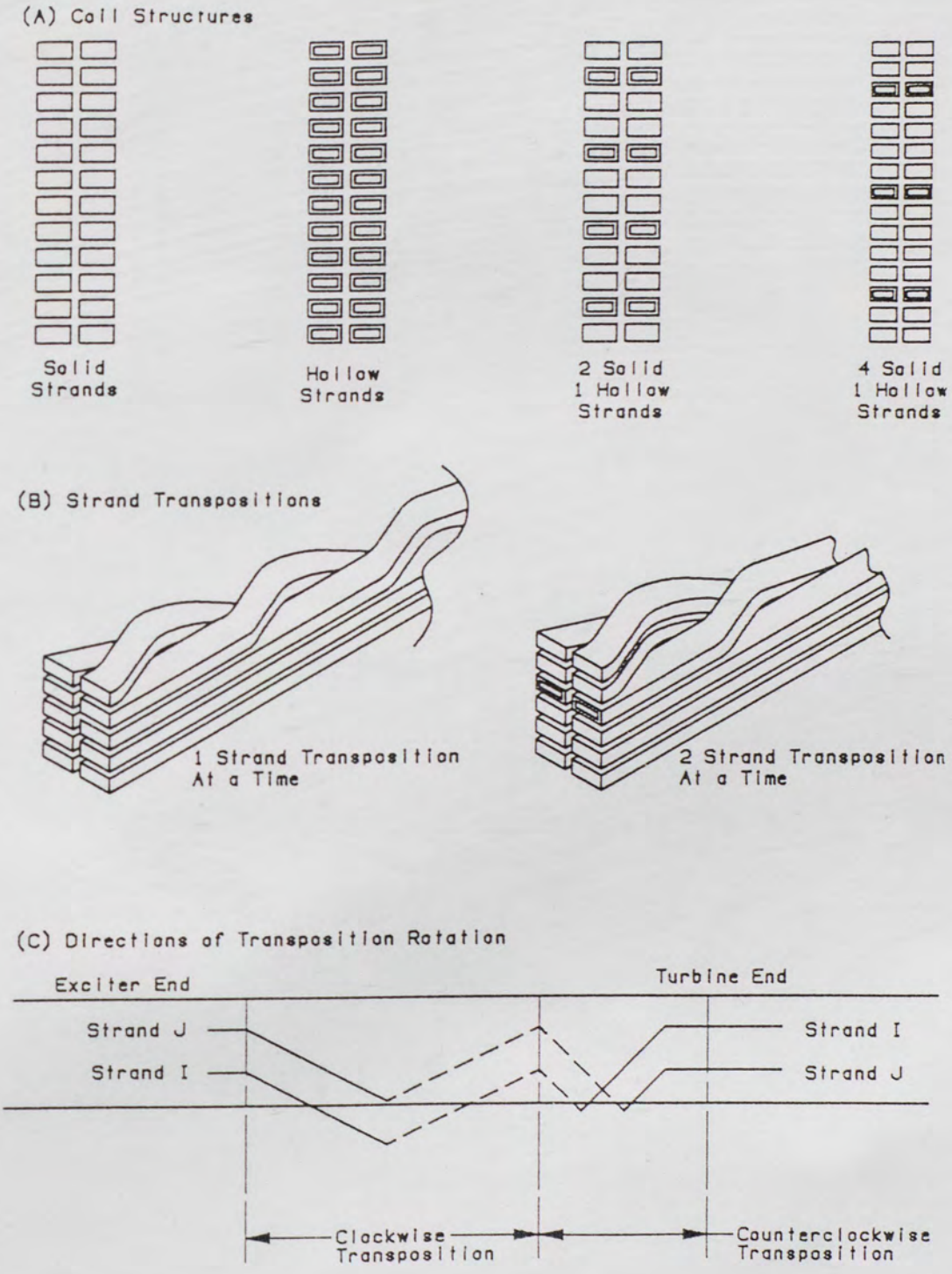

FIGURE 9. Examples of Coil Structures and Transpositions

locations in the roebel bar. All data describing this strand movement is part of the program input. Figure 10 shows the movement of the strand. For multi roebel bar coils, the strand number is defined as in Figure 11.

To determine the circulating currents between strands in a roebel bar, this paper assembles and solves a set of voltage difference equations for each pair of successive strands [12]. The equations are based on a model of the roebel bar convenient to computerized equation assembly for various transposition patterns. The path of an individual strand is approximated by a succession of axial moves between crankovers and radial moves at crankovers shown by a dashed line in Figure 12. The strands are shown not transposed in the end regions in this figure. This, however, is not a limitation of this analysis. The user can input the transposition data for the end regions as well as for the slot region.

In addition to the approximation described above, the following general assumptions are made in the analysis:

1. Permeability of stator core is infinite.
2. Only the fundamental frequency component of the current and flux is considered.
3. The effect of the radial flux which penetrates into a coil in the slot and the coil end regions is not considered.
4. Other assumptions will be describe as needed.

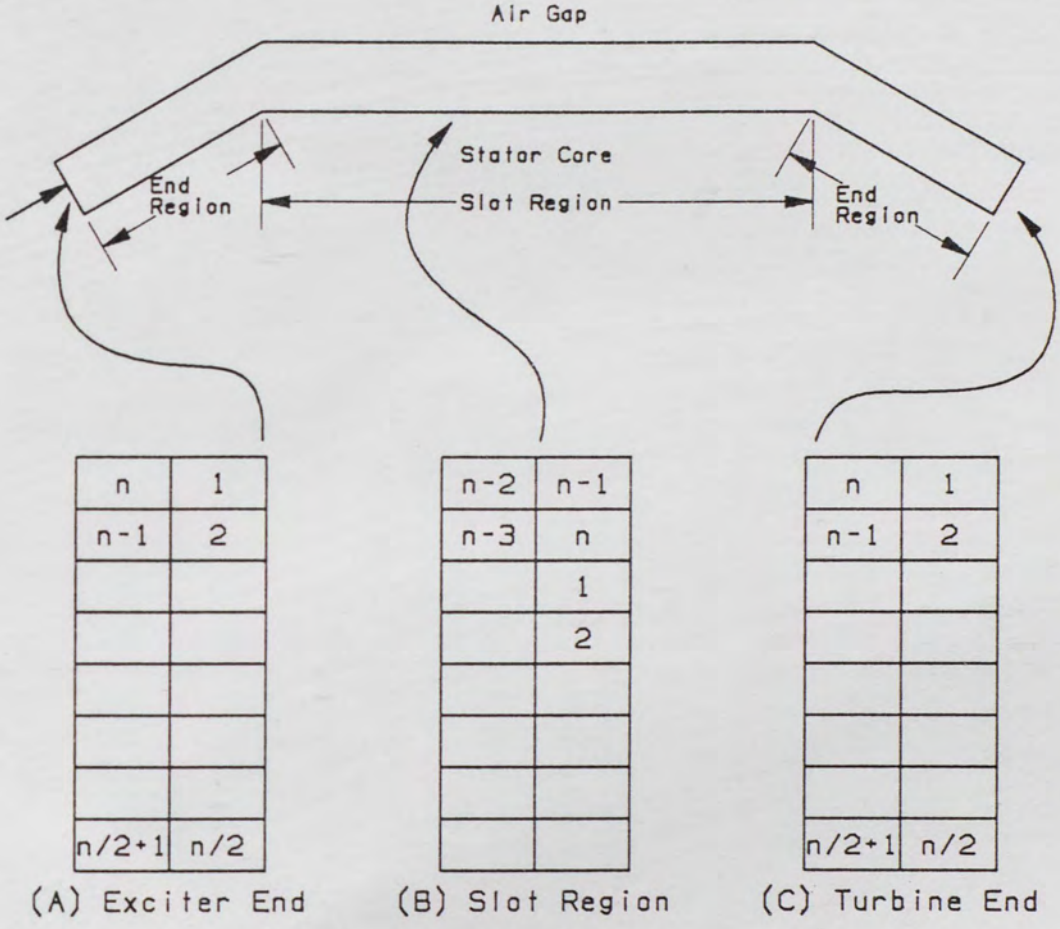

(1) Cross section of one roebel bar viewed from the exciter end

(2) "n" is the number of strands in one roebel bar.

FIGURE 10. Movement of the Strands with the Advancement along the Coil
(In case of 360 degree transposition in the slot region with one strand at a time roebels)

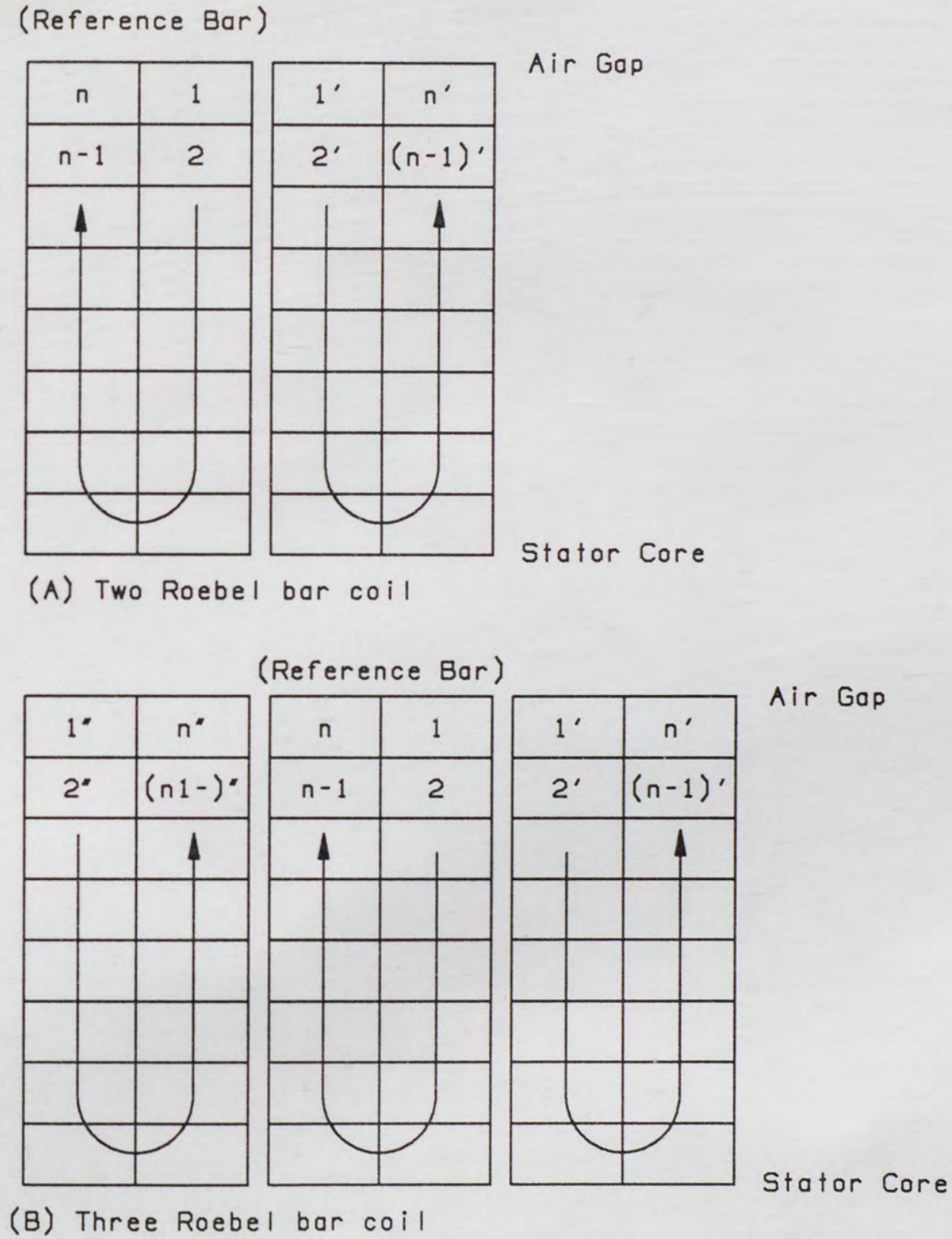

FIGURE 11. Strand Number at Exciter End
(View from Exciter End)

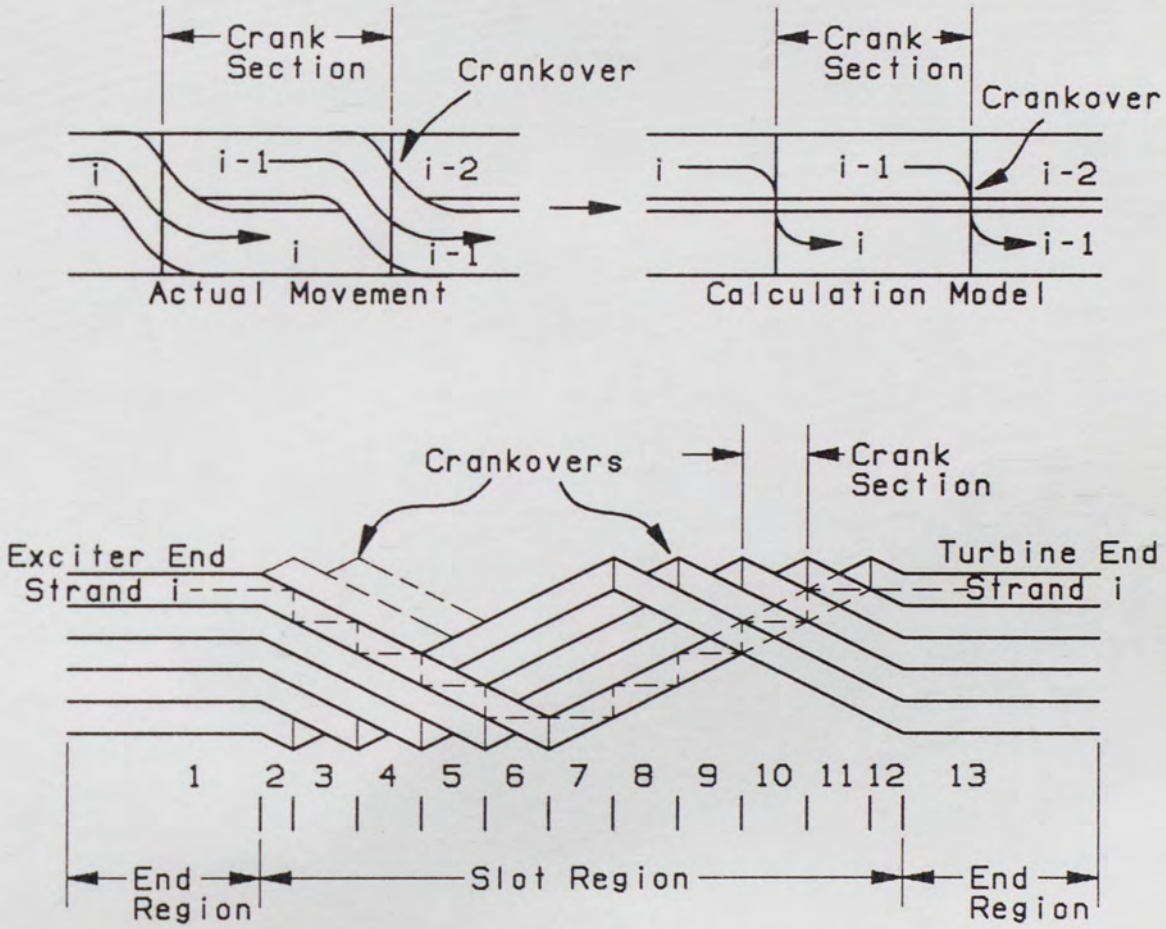

The numbers along the coil side mean crank section number. The dashed line indicates the path of the strand in the calculation.

FIGURE 12. Calculation Model of Strand Path

VOLTAGE DIFFERENCE EQUATIONS

The voltage equations between ends of the coil strands consists of three parts, that is, V_{END1} for the coil end region of exciter side, V_{SLOT} for the stator slot region, and V_{END2} for the coil end region of the turbine side, and they are given below (Figure 13) [10,12].

$$\begin{aligned} V_1 &= V_{1END1} + V_{1SLOT} + V_{1END2} = R_1 \cdot I_1 + jX_{11} \cdot I_1 + jX_{12} \cdot I_2 + \ldots + jX_{1i} \cdot I_i + \ldots + jX_{1n} \cdot I_n + E_1 \\ V_i &= V_{iEND1} + V_{iSLOT} + V_{iEND2} = R_i \cdot I_i + jX_{i1} \cdot I_1 + jX_{i2} \cdot I_2 + \ldots + jX_{ii} \cdot I_i + \ldots + jX_{in} \cdot I_n + E_i \\ V_n &= V_{nEND1} + V_{nSLOT} + V_{nEND2} = R_n \cdot I_n + jX_{n1} \cdot I_1 + jX_{n2} \cdot I_2 + \ldots + jX_{ni} \cdot I_i + \ldots + jX_{nn} \cdot I_n + E_n \end{aligned} \quad (1)$$

where V, I, and E are phasor quantities, and

R_i: Resistance of strand i

X_{ii}: Self-reactance of strand i

X_{ij}: Mutual-reactance between strand i and strand j in coil

I_i: Current in strand i

$j = \sqrt{-1}$

V_i: Voltage between ends of strand i

E_i: Electromotive force in strand i

For top coil, the electromotive force is produced by the fluxes from the other coils in the end regions and from the bottom coil in the slot region. For bottom coil, the electromotive force is produced by the fluxes from the other coils in the end regions.

In equation 1, mutual reactances between strands in the top coil and strands in the bottom coil do not appear. The flux linkage between these coils is treated as the electromotive force in the top coil strand.

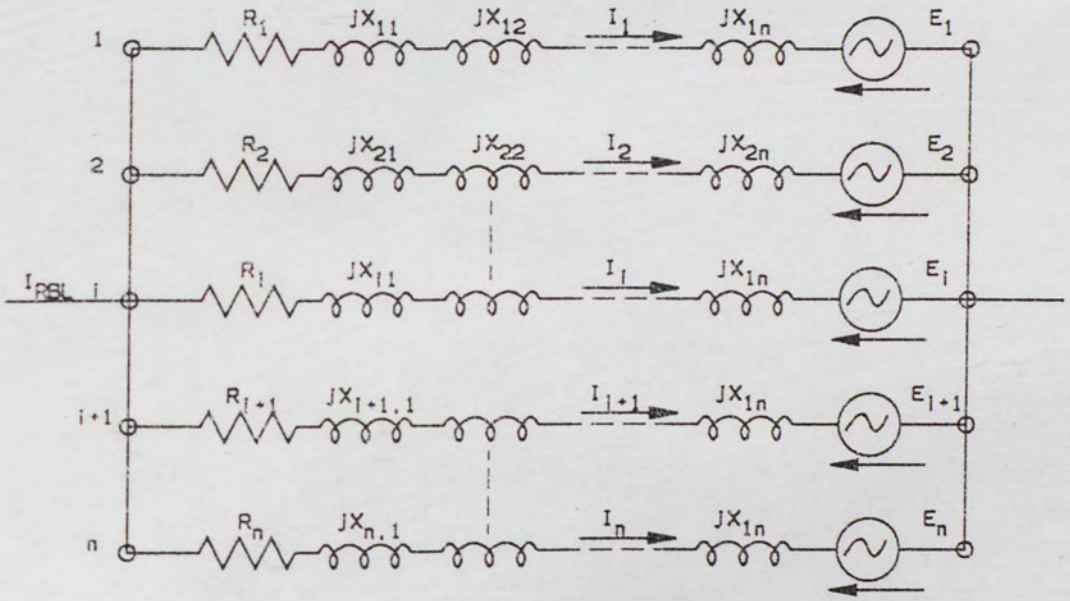

FIGURE 13. Electrical Circuit in a Coil Side

Resistance is given below.

$$R_i = \rho_i \frac{l_i}{S_i} \quad (2)$$

where,

ρ_i : Resistivity of strand material

l_i : Length of strand i. It is assumed that the length of strand i is equal to the length of the coil side.

S_i : Cross section area of strand i

Voltage difference equations between successive strands are determined as follows from Equation 1.

$$\begin{aligned} V_1 - V_2 &= R_1 \cdot I_1 - R_2 \cdot I_2 + j(X_{11} - X_{21}) \cdot I_1 + \ldots + j(X_{1n} - X_{2n}) \cdot I_n + E_1 - E_2 \\ V_i - V_{i+1} &= R_i \cdot I_i - R_{i+1} \cdot I_{i+1} + j(X_{i1} - X_{i+1,1}) \cdot I_1 + \ldots + j(X_{in} - X_{i+1,n}) \cdot I_n + E_i - E_{i+1} \\ V_{n-1} - V_n &= R_{n-1} \cdot I_{n-1} - R_n \cdot I_n + j(X_{n-1,1} - X_{n1}) \cdot I_1 + \ldots + j(X_{n-1,n} - X_{n,n}) \cdot I_n + E_{n-1} - E_n \end{aligned} \quad (3)$$

Then both ends of a coil are short-circuited,

$$V_i - V_{i+1} = 0 \quad (4)$$

In addition to the above (n-1) voltage difference equations, the following current equation must be satisfied:

$$I_1 + I_2 + \ldots + I_n = I_{RBL} = \frac{I_{COIL}}{N_{RBL}} \quad (5)$$

where,

I_i : Current in strand i

I_{RBL} : Roebel bar current

I_{COIL} : Coil current

N_{RBL} : The number of Roebel bars in one coil side

Equations 3 and 5 are written below in matrix form.

$$[Z] \cdot [I] = [V] - [E] + [I_{COIL} / N_{RBL}] \quad (6)$$

where,

$$[I] = \begin{bmatrix} I_1 \\ I_i \\ \cdots \\ I_n \end{bmatrix} \qquad [V] = \begin{bmatrix} 0 \\ 0 \\ \cdots \\ 0 \end{bmatrix}$$

$$[E] = \begin{bmatrix} E_1 - E_2 \\ E_i - E_{i+1} \\ \cdots\cdots\cdots \\ E_{n-1} - E_n \\ 0 \end{bmatrix} \qquad [I_{COIL} / N_{RBL}] = \begin{bmatrix} 0 \\ 0 \\ \cdots \\ I_{COIL} / N_{RBL} \end{bmatrix} \quad (7)$$

Impedance matrix, which is the largest matrix in the program, is shown on the next page (Figure 14). Equation 6 will be solved by Gaussian Elimination Method [10].

CALCULATION OF REACTANCE IN SLOT REGION

Calculation of strand reactances in the slot region to set the impedance matrix [Z] is explained here. Assuming the cross slot flux in the slot region goes straight across the slot, self-reactance of strand i is determined by the area above strand i in an axial/radial

$[Z] =$

R_1 $+j(X_{11}-X_{21})$	$-R_2$ $+j(X_{12}-X_{22})$	. . .	. . .	.	$j(X_{1,n}-X_{2,n})$
$j(X_{2,1}-X_{3,1})$	R_2 $+j(X_{22}-X_{32})$	. .		. .	. . .
. . .	. . .			.	. . .
		. .	R_i $+j(X_{ii}-X_{i+1,i})$	. . .	
. .	. .			.	. .
$j(X_{n-1,1}-X_{n,1})$	$j(X_{n-1,2}-X_{n,2})$	. .	. . .		$-R_n$ $+j(X_{n-1,n}-X_{nn})$
1	1	. .	. . .	.	1

FIGURE 14. Impedance Matrix

plane through the length of a stator core. Then, mutual-reactance between strand i and strand j is determined by the mutual area above strand i and strand j.

Reactances are given below.

$$X_{ii} = \omega \frac{u_o \bullet A_{ii}}{B_s \bullet 10^8}$$

$$X_{ij} = \omega \frac{u_o \bullet A_{ij}}{B_s \bullet 10^8}$$

where,

X_{ii} : Self-reactance

X_{ij} : Mutual-reactance

ω : Angular frequency

u_o : Permeability of free space

B_s : Slot width

A_{ii} : Area above strand i (see Figure 15)

A_{ij} : Mutual area above strand i and strand j (see figure 15)

Thus the problem reduces to calculation of area [13]. In this program the location of the strands is determined at each crank section, then the area is calculated from product of the length of the crank section and the location of the strands. The areas at all crank sections are summed up along the length of the stator core.

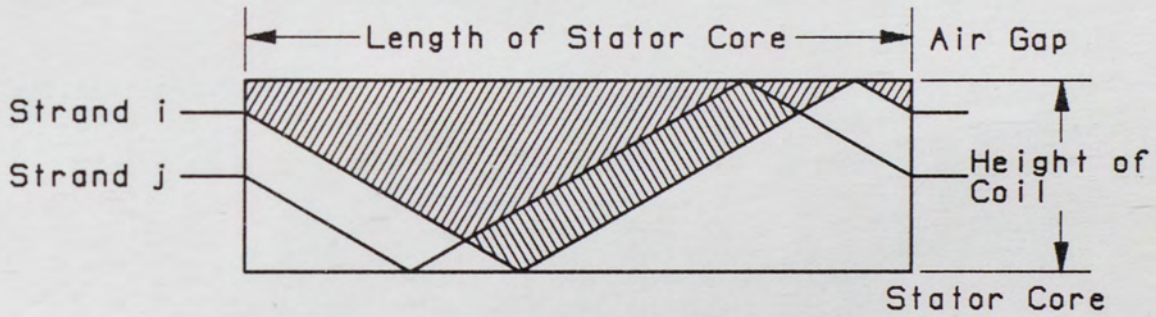

A_{ii} = ▨ + ▨

A_{ij} = ▨

FIGURE 15. Area to Determine X_{ii} and X_{ij}

CALCULATION IN END REGION

The flux pattern along the coil height in the end regions is assumed like in Figure 16. Flux consists of the average component B_o and the variable component shown in the middle part of Figure 16. The variable component of the flux was divided into two components in the computer program.

Assuming average flux density B_o, then B_T in Figure 16 is given below.

$$B_T = B_o + \frac{K}{2} \cdot (P_{COIL} + jQ_{COIL})$$

where,

$K = \frac{u_o}{B_E}$: Constant term

B_E : Distance between centerlines of two adjacent coils (see Figure 16)

P_{COIL} : Real part of the coil current.

Q_{COIL} : Imaginary part of the coil current.

Average flux density at each crank-section in the end regions has to be input. Hence, the flux density B_i which produces the emf between consecutive strand i and strand i+1 is expressed as follow.

$$B_i = B_o + \frac{K}{2}(P_{COIL} + jQ_{COIL}) - \frac{K\sum_i I_i + K\sum_{i+1} I_{i+1}}{2} \cdot N_{RBL} \qquad (8)$$

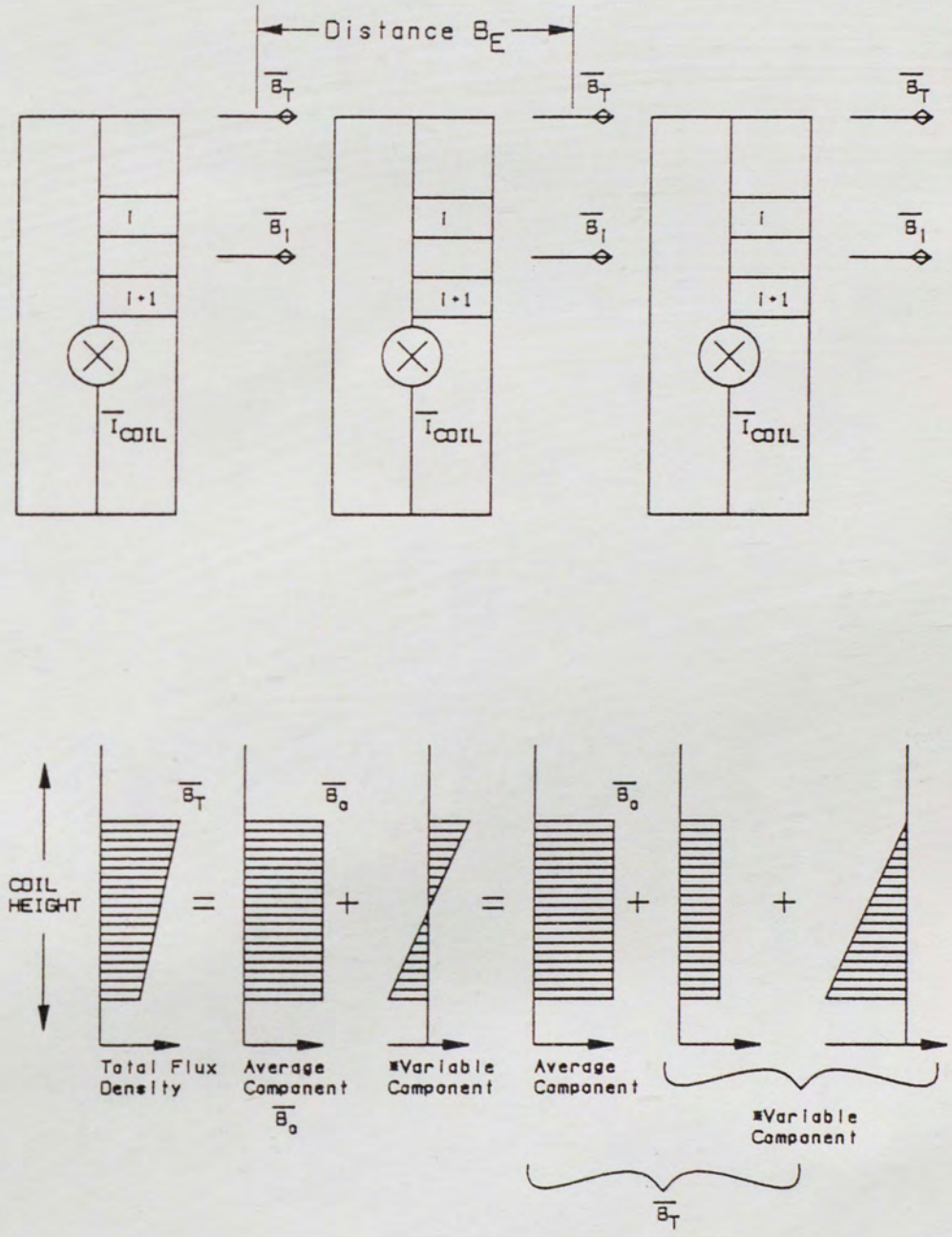

FIGURE 16. Flux Pattern in End Regions Along Coil Height

From Figure 17, $K\sum_1 I_1 = K(I_3 + I_1)$ and $K\sum_2 I_2 = K(I_3 + I_1 + I_4 + I_5)$. In general, $K\sum_i I_i$ is K time the sum of currents in strands above strand i, including strand i, and $K\sum_{i+1} I_{i+1}$ is K time the sum of currents in strands above strand i+1.

The voltage difference equation between strand i and strand i+1 consists of three parts, that is, the exciter end part, the slot part, and the turbine part. The voltage difference equation in the end regions is given below instead of the use of the reactances.

$$V_i - V_{i+1} = -jCB_i \qquad (9)$$

where,

$$C = \Delta H \cdot L_{END} \cdot \frac{\omega}{10^8}$$

ΔH : Distance between two consecutive strand i and strand i+1. ΔH is positive when strand i locates above stand i+1.

L_{END} : Length of the transposition section in the end region.

ω : Angular frequency.

Substituting equation 9 into equation 3,

$$\{V_{iEND1} - V_{i+1END1}\} + \{V_{iSLOT} - V_{i+1SLOT}\} + V_{iEND2} - V_{i+1END2}\} = -jCB_{END1} + \{R \cdot I_i - R_{i+1} \cdot I_{i+1} + j(X_{i1} - X_{i+1,1}) \cdot I_1 + \ldots + j(X_{in} - X_{i+1,n}) \cdot I_n\} - jCB_{END2}$$

(10)

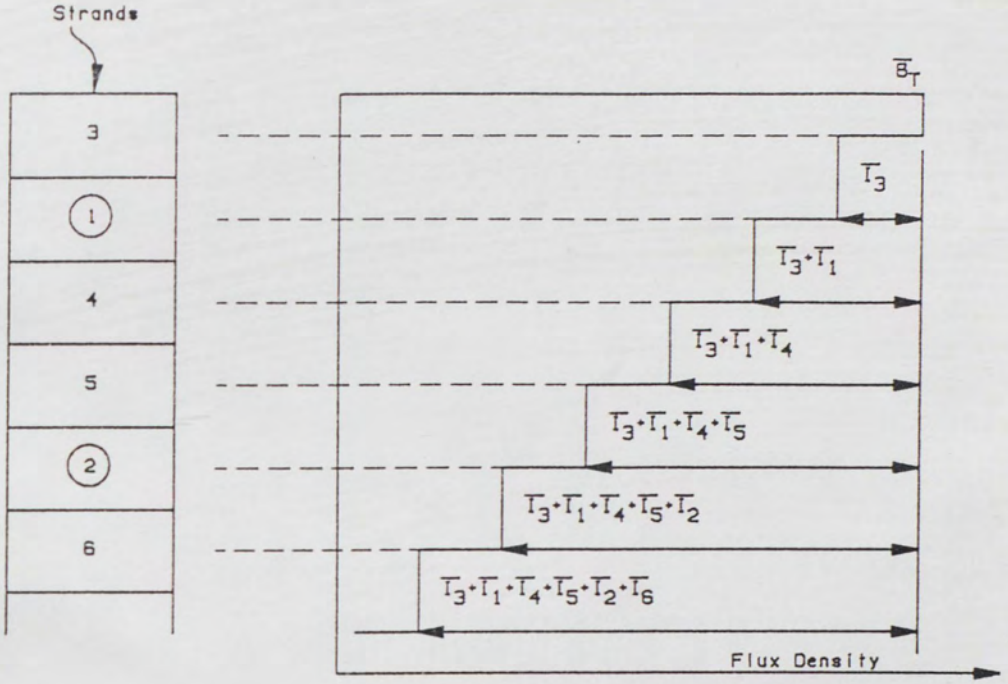

$$B_1 = B_o + \frac{K}{2}(P_{COIL} + Q_{COIL}) - \frac{K(I_3 + I_1) + K(I_3 + I_1 + I_4 + I_5)}{2} \cdot N_{RBL}$$

FIGURE 17. Simple Example of Flux Density in End Region

In the above equation, reactances $X_{i,1},\ldots,X_{i+1,n}$ have slot reactances only. Substituting equation 8 into equation 10 the voltage equation for the ends is:

$$R_i \cdot I_i - R_{i+1} \cdot I_{i+1} + j(X_{i1} - X_{i+1,1}) \cdot I_1 + \ldots + j(X_{i,n} - X_{i+1,n}) \cdot I_n = \{jCB_o + jC\frac{K}{2}(P_{COIL} + jQ_{COIL}) - jCN_{RBL}\frac{K\sum_{i} I_i + K\sum_{i+1} I_{i+1}}{2}\}_{END1} + \{jCB_o + jC\frac{K}{2}(P_{COIL} + jQ_{COIL}) - jCN_{RBL}\frac{K\sum_{i} I_i + K\sum_{i+1} I_{i+1}}{2}\}_{END2}$$

Thus,

$$R \cdot I_i - R_{i+1} \cdot I_{i+1} + j(X_{i1} - X_{i+1,1}) \cdot I_1 + \ldots + j(X_{i,n} - X_{i+1,n}) \cdot I_n + jCN_{RBL}\frac{\{K\sum_{i} I_i + K\sum_{i+1} I_{i+1}\}_{ED1}}{2} + jCN_{RBL}\frac{\{K\sum_{i} I_i + K\sum_{i+1} I_{i+1}\}_{END2}}{2} = \{jCB_o + jC\frac{K}{2}(P_{COIL} + jQ_{COIL})\}_{END1} + \{jCB_o + JC\frac{K}{2}(P_{COIL} + jQ_{COIL})\}_{END2}$$

This gives the complete reactance equation for the exciter end, slot region, and turbine end as seen in Figure 18.

STRAND INDUCED VOLTAGE

These voltages are produced in the end regions and in the slot region by the flux from other coils. In this program, the induced voltages are calculated by Faraday's Law (Figure 19). Electromotive force is given below [3].

$$e = -N\frac{d\phi}{dt}$$

$[Z] =$

. . .	$R_i + j(X_{ii} - X_{i+1,i})$ $+ jCN_{RBL}\frac{\{K\sum_{i} I_i + K\sum_{i+1} I_{i+1}\}_{END1}}{2}$ $+ jCN_{RBL}\frac{\{K\sum_{i} I_i + K\sum_{i+1} I_{i+1}\}_{END2}}{2}$	. . .
1	. . .	1

FIGURE 18. Complete Impedance Matrix

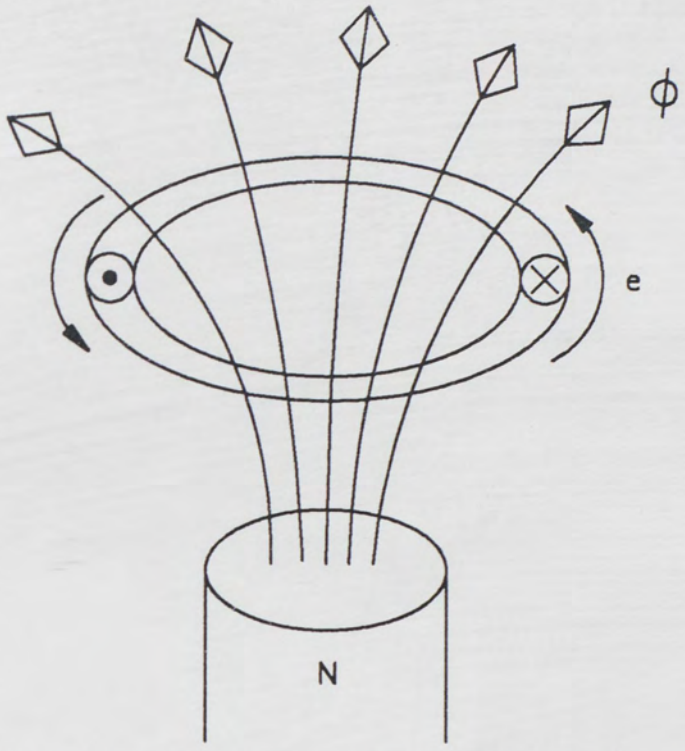

(A) Directions of Flux and Electromotive Force

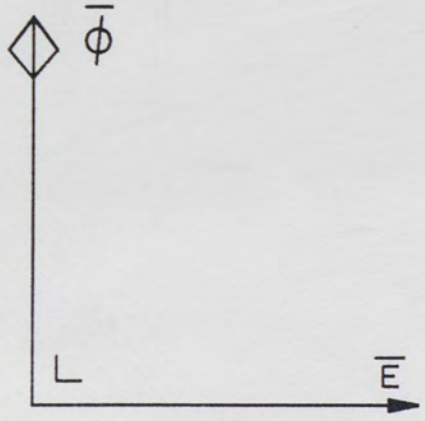

(B) Phasor Diagram

FIGURE 19. Faraday's Law

where,

e: Electromotive force

N: Number of turns

ϕ : Flux linking coil

t: Time

Figure 20 shows the simplified model to explain the directions of the flux, current, and electromotive force in two consecutive strands.

$$V_i = R_i \cdot I_i + E_i$$
$$V_{i+1} = R_{i+1} \cdot I_{i+1} + E_{i+1}$$
$$V_i - V_{i+1} = (R_i \cdot I_i - R_{i+1} \cdot I_{i+1}) + (E_i - E_{i+1}) = (R_i \cdot I_i - R_{i+1} \cdot I_{i+1}) - jC \cdot \Delta B$$

Strand i and strand i+1 are short circuited. So, the above equation is:

$$(R_i \cdot I_i - R_{i+1} \cdot I_{i+1}) - jC \cdot \Delta B = 0$$

The strand induced voltage is defined as the voltage produced by the flux from other coils. ΔB is independent of the strand currents I_i and I_{i+1}. Thus, the equation is given below.

$$R_i \cdot I_i - R_{i+1} \cdot I_{i+1} = jC \cdot \Delta B$$

In this program, strand induced voltages are calculated at each crank section, and they are added vectorially through the whole length of the coil side [14].

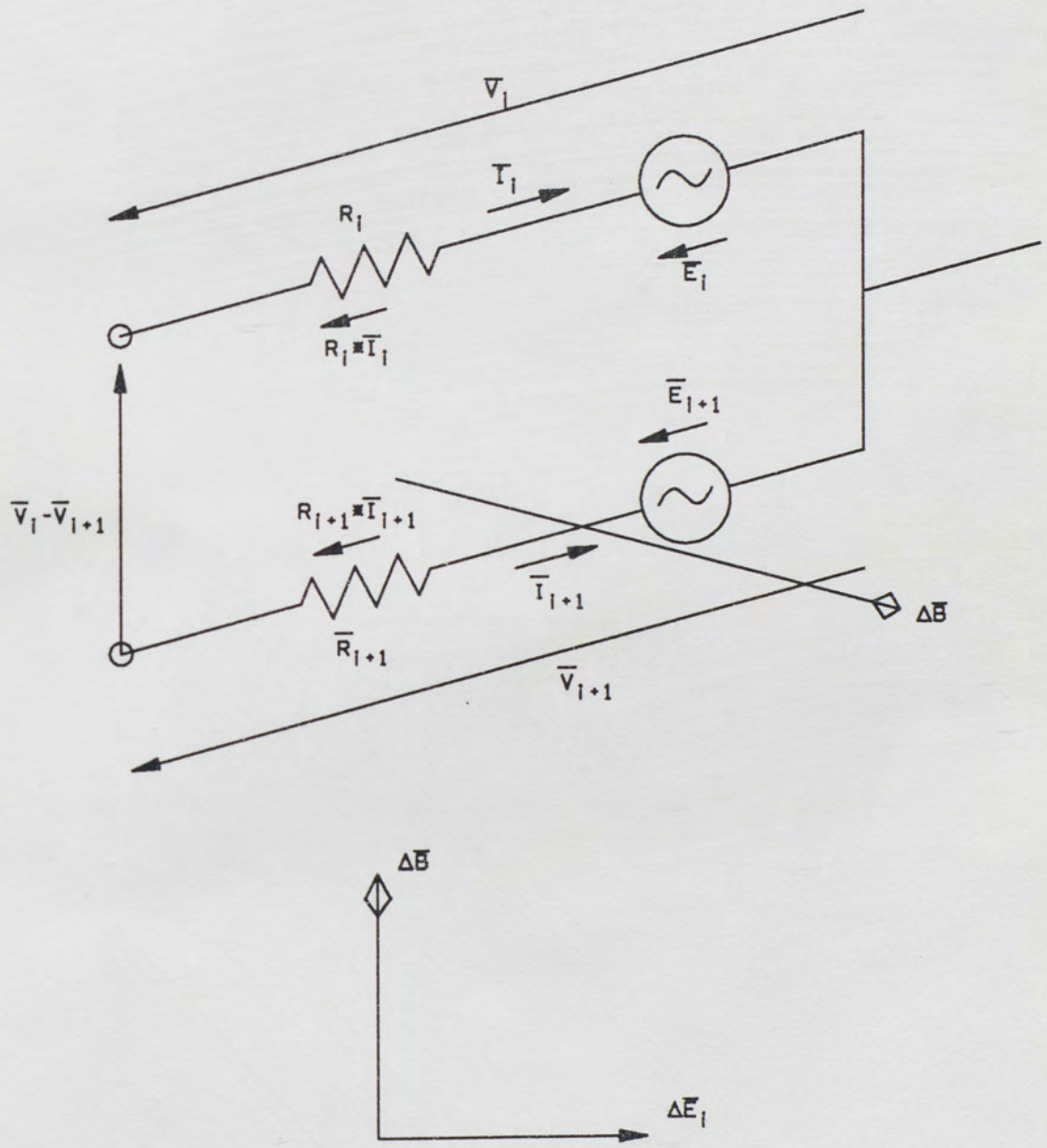

FIGURE 20. Simplified Model for Voltage Difference Equation

Stand induced voltages are produced in the end regions and also in the slot region. The flux densities needed for calculation in the end regions have to be supplied by the program user. RMS value of the flux densities should be used in this program.

In the slot region cross slot flux produces the voltage. As mentioned in chapter 2, the typical method of calculating the cross slot flux is as follows [5]:

$$B_{CS} = u_o \bullet \frac{I_{BOT}}{B_S}$$

where,

B_{CS} : Cross slot flux in RMS value

I_{BOT} : Current of bottom coil in RMS value

u_o : Permeability of free space

B_s : Slot width

To more accurately account for the voltage induced by cross slot flux, the cross slot flux equation developed in chapter 2 will be used:

$$B_{SAME} = B_o \cdot (1 + \frac{x_i}{HC})$$

where,

B_O=B_{CS}

HC= height of top stator coil.

x_i= radial height of i^{th} strand.

In the slot region, the voltage is produced only in the top coil, because there is no flux excited by the top coil that penetrates the bottom coil [10]. Figure 21 shows these fluxes used in the program of the deep bar effect.

Figure 22 shows the phasor diagram of the electromotive forces in top and bottom coils. Phasors representing fluxes in the end regions are drawn in arbitrary directions just for explanation purpose. Resultant electromotive force in the top coil is the sum of the voltages in the end regions and in the slot region. Resultant electromotive force in the bottom coil, however, is the sum of the voltages in the end regions. In Figure 22, it was assumed that the end region fluxes in the exciter end and the turbine end regions had the same phase. This assumption is not required by the program. The user can input different end region fluxes for the exciter end and the turbine end regions.

Equation 6 is solved by Gaussian Elimination to determine the individual strand currents *[I]*. As shown in equation 5, all the strand currents in a roebel bar add together to equal load current. However, some strands may have twice the RMS current of another strand, therefore, causing a localized hot spot in the stator coil. This is a major factor not accounted for in past loss calculation methods. It is the intent of this thesis to improve the flux and loss calculation to more accurately calculate these localized hot spots in stator coils.

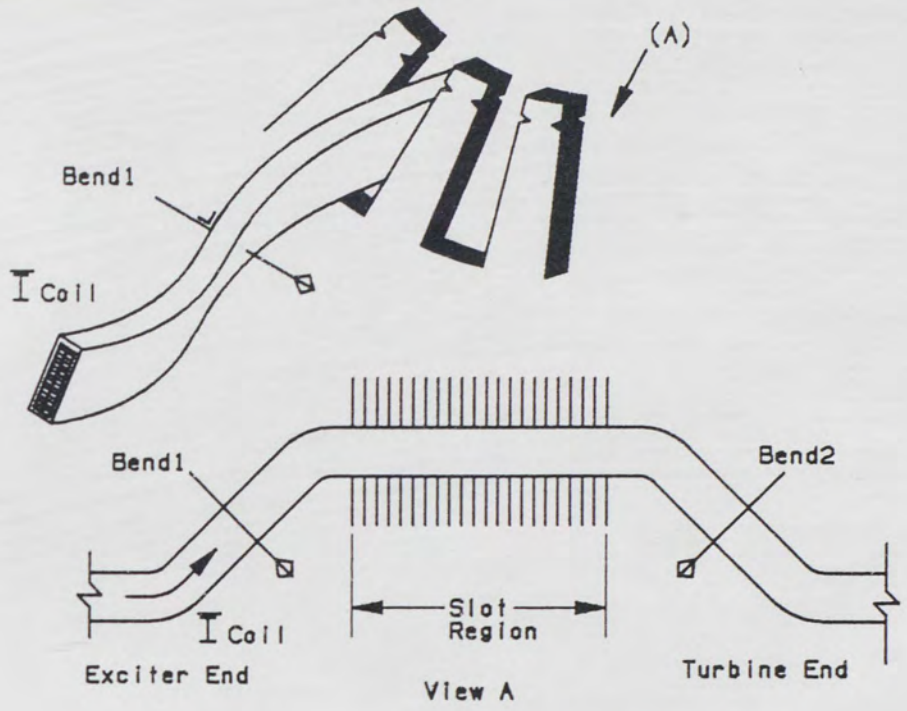

(A) End Regions

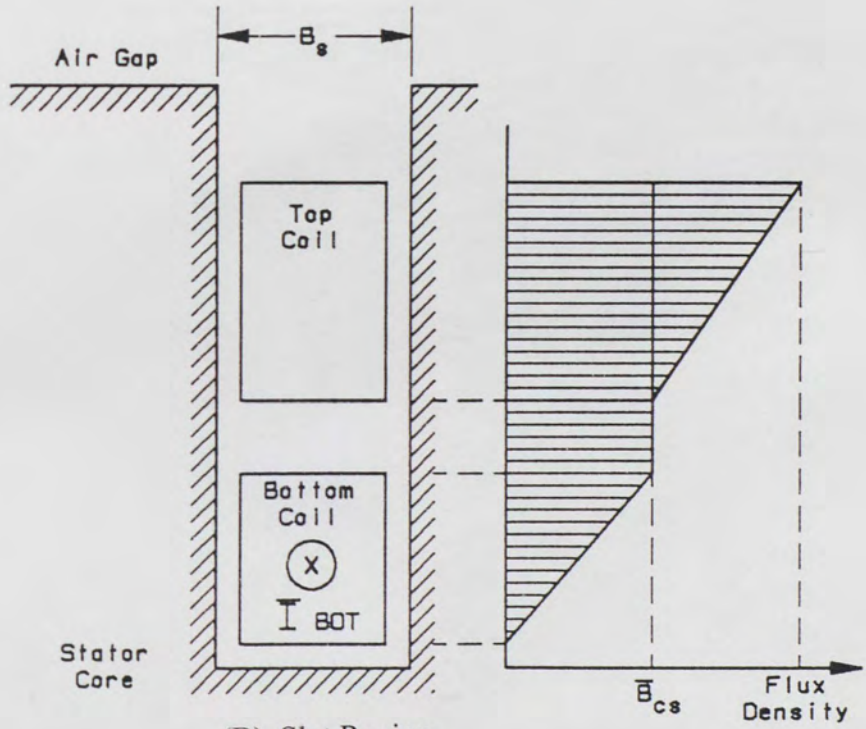

(B) Slot Region

FIGURE 21. Fluxes in End Regions and in Slot Region

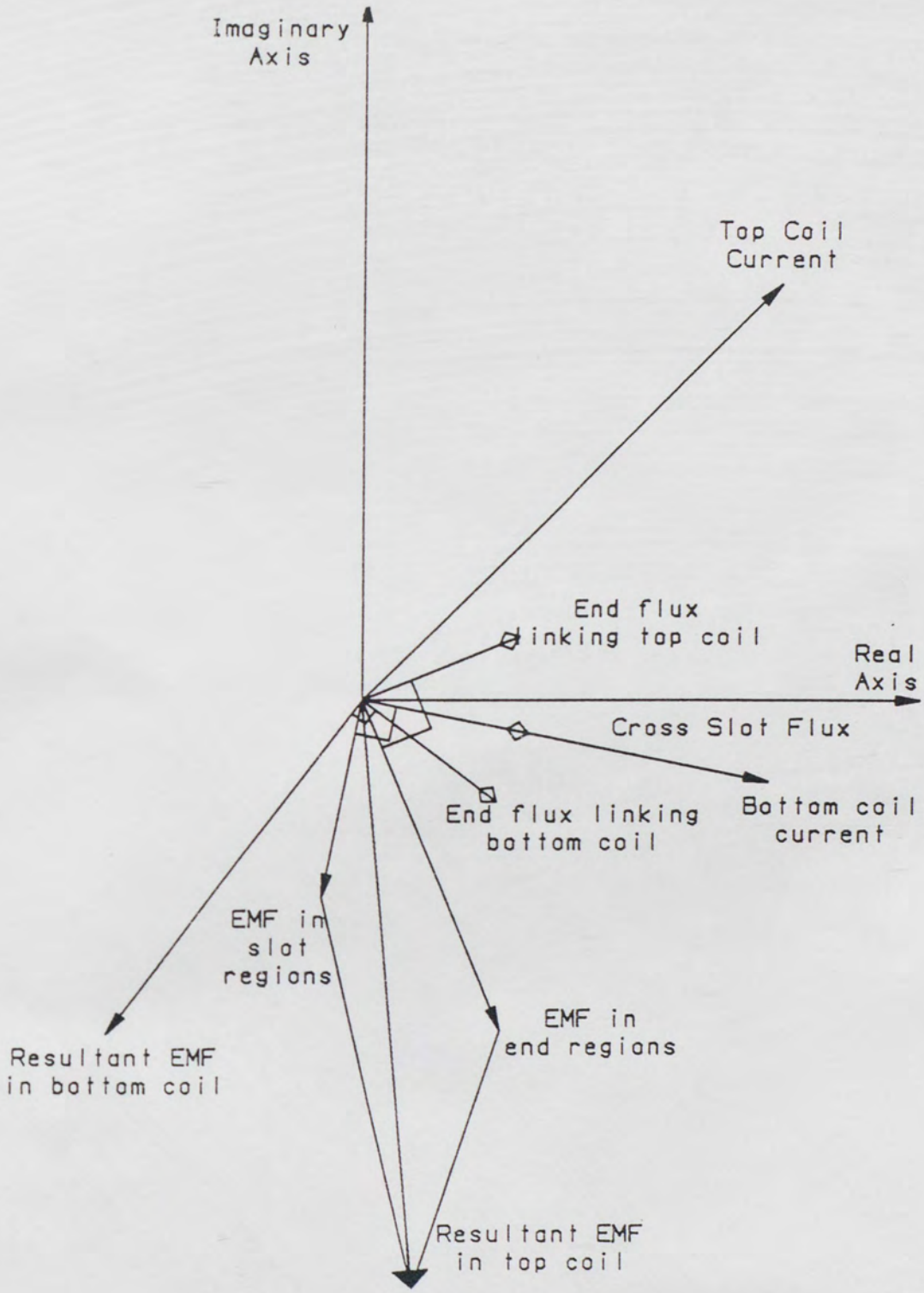

FIGURE 22. Phasor Diagram of Electromotive Force

IV. PROGRAM STRUCTURE

This program consists of one main program and seven subprograms. Main features of each program are described below.

1. Main Program:

Main program reads input data, calculates strand resistances, sets matrices, calls necessary subprograms, calculates strand currents and finally outputs the results.

2. Subprogram STRLOC:

This subprogram sets matrices which describe the strand location in the coil at each crank section.

3. Subprogram STRXS:

This subprogram calculates self and mutual reactances of strands at each crank section in the slot region.

4. Subprogram STRXE:

This subprogram calculates the reactances for the end regions and sets these reactances into appropriate locations of the matrix *[Z]*.

5. Subprogram STRVOL:

This subprogram calculates induced voltage between two consecutive strands and sets matrices. The results of the induced voltage calculation are stored in these vectors.

6. Subprogram SOLVER:

This subprogram solves the complex simultaneous voltage difference equations.

7. Subprogram CSLOSS:

This subprogram calculates the cross slot flux and its associated losses in each strand.

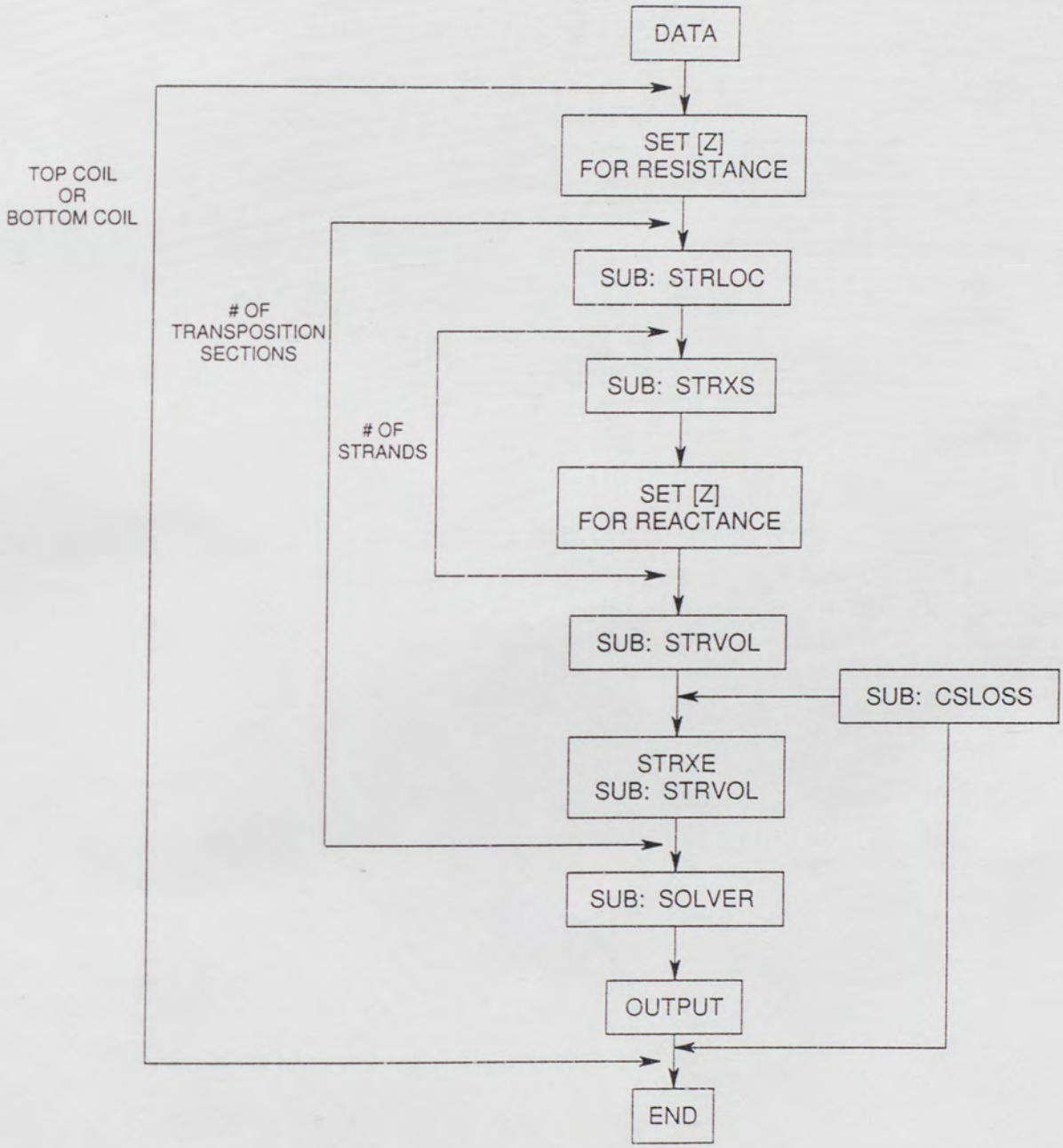

FIGURE 23. Flowchart

CALCULATION VS TEST VALUES

This chapter demonstrates the validity of the methods discussed in this thesis by comparing the results calculated by the program described in the previous chapter to those measured during factory test. The program uses individual strand currents, and cross slot internal strand losses to determine the total cross slot flux losses. These losses together with the additional losses calculated by other programs (I^2R) are inputs into a temperature calculation program. This temperature program calculates the temperature for each strand and vent tube in the stator coil.

Thermocouples were placed at the end of the core and the end of the coil since these are usually the hottest spots in the coil [15]. The end of the core is a potential hot spot because the strand loss intensity is the highest in the slot, and the end of the coil is a potential hot spot because the gas is the hottest at this point which in turn pushes the copper temperature up. In addition to these two potential hot spots, five other thermocouples were placed at various axial lengths throughout the coil to develop a more accurate temperature profile for validating the calculation. All axial locations are referenced from the Exciter End.

Top coil axial thermocouple locations: 142",211",216",220",224",263",291"

Bottom coil locations: 145",208",218",221",266",286",291.5"

Three thermocouples were placed at each axial location mentioned above. Of the three thermocouples, one was placed on the top left strand, one on the top vent tube, and one on the top right strand (Figure 24). Thermocouples were installed at the same axial locations in slots 14 and 16. Temperatures in these two slots were expected to be approximately identical because top and bottom coil currents in both slots were in phase (all 4 coils were in the same phase group). Because of the redundant thermocouples (two slots vs one), there was a great deal of confidence in the tested data.

The AC synchronous generator tested was hydrogen inner-cooled, single tube stack, 720° roebel transposition, rated at 285 MVA, 20KV, .85 power factor. The test was conducted under both short circuited and open circuited conditions with cold gas temperature of 46°C at 60 psig. Before the test, the ambient temperatures were recorded and stator coil resistances were measured to ensure proper I^2R loss calculations.

Tables 1 and 2 show the tested values for open circuit and short circuit tests in slot 16. The calibrated full load temperatures were tabulated using the short circuit and open circuit test data per IEEE test procedures for synchronous machines. Figures 25 through 30 show that the thermocouple readings in slot 14 were within 2°C for top coils and 5°C for bottom coils. Therefore, it is assumed that all thermocouples were reliable and reading correctly.

Initially, the full load calculated data using the present (traditional) loss calculation methods was compared to the calibrated full load test data. The maximum temperature

difference between the calibrated test values and the calculation values (traditional method) was found to be over 20°C (Table 3).

The loss calculations were repeated using the improved methods described in this thesis. The calibrated full loss test values compared to these new calculated full load test values showed significantly more accurate results. Temperature differences between test and calculated data for the top coils was less than 5°C; and less than 10°C for the bottom coils (Tables 4-7). Most data points in the bottom coils were within 5°C but one value showed approximately a 10°C difference. The exact reason for this rather significant discrepancy in the bottom coil has not been determined at this time. However, this discrepancy could be because of inconsistencies during manufacturing or assembly.

Figures 25 through 30 show the close temperature profile between test data and the calculated data (using improved loss calculation methods described in this thesis).

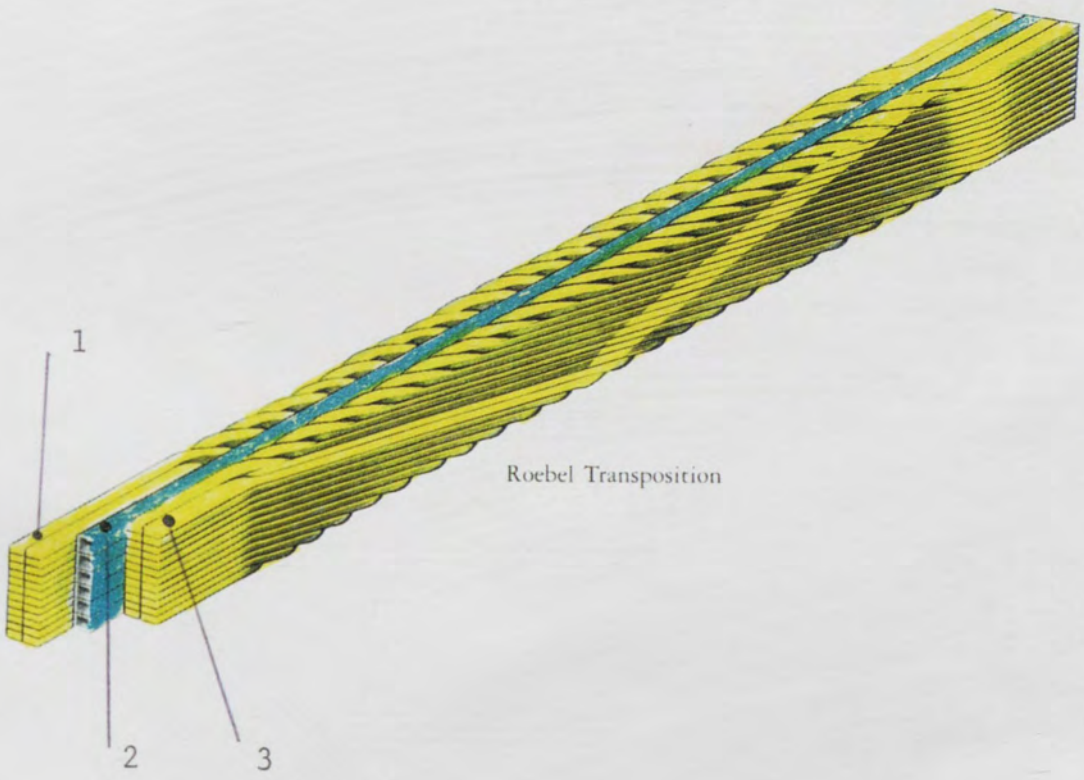

FIGURE 24. Thermocouple Locations
(1 for top left strand, 2 for top vent tube, 3 for right top strand)

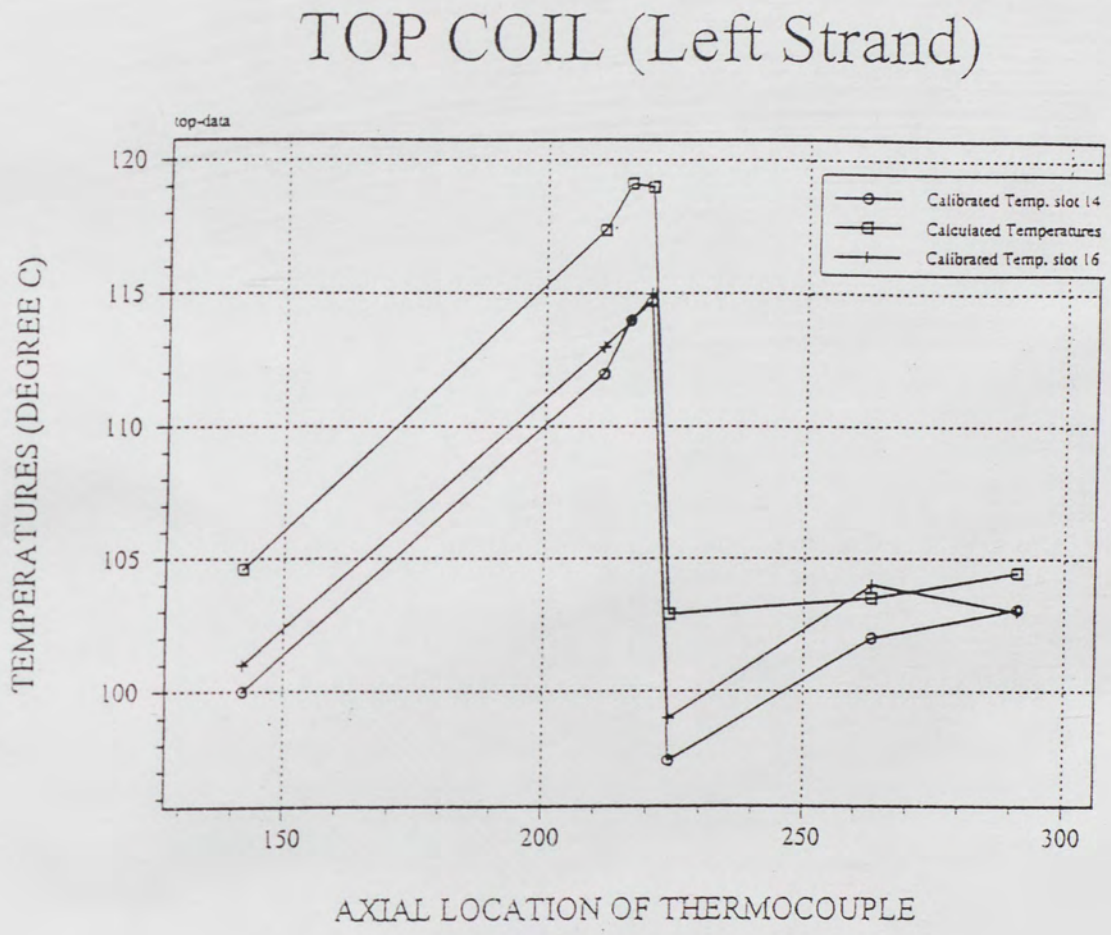

FIGURE 25. Top Coil Left Strand Temperature Profile

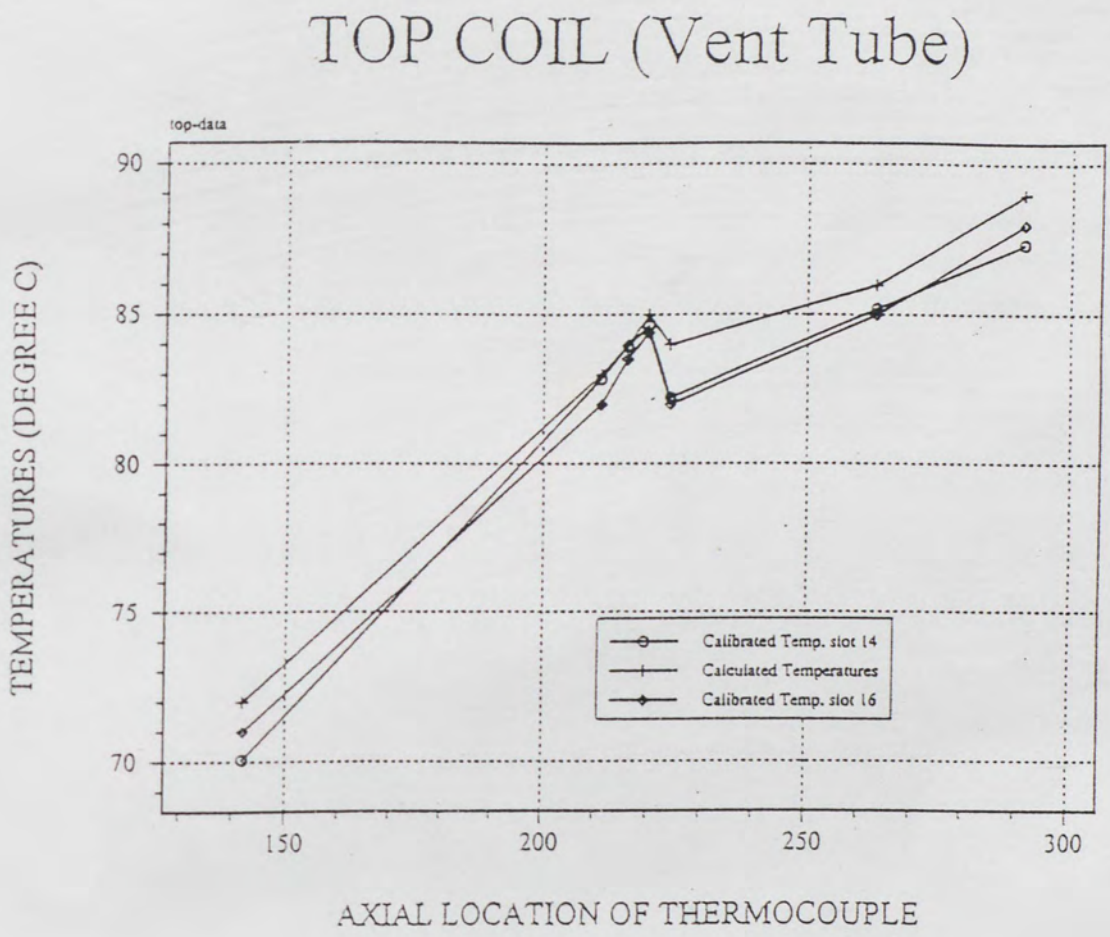

FIGURE 26. Top Coil Vent Tube Temperature Profile

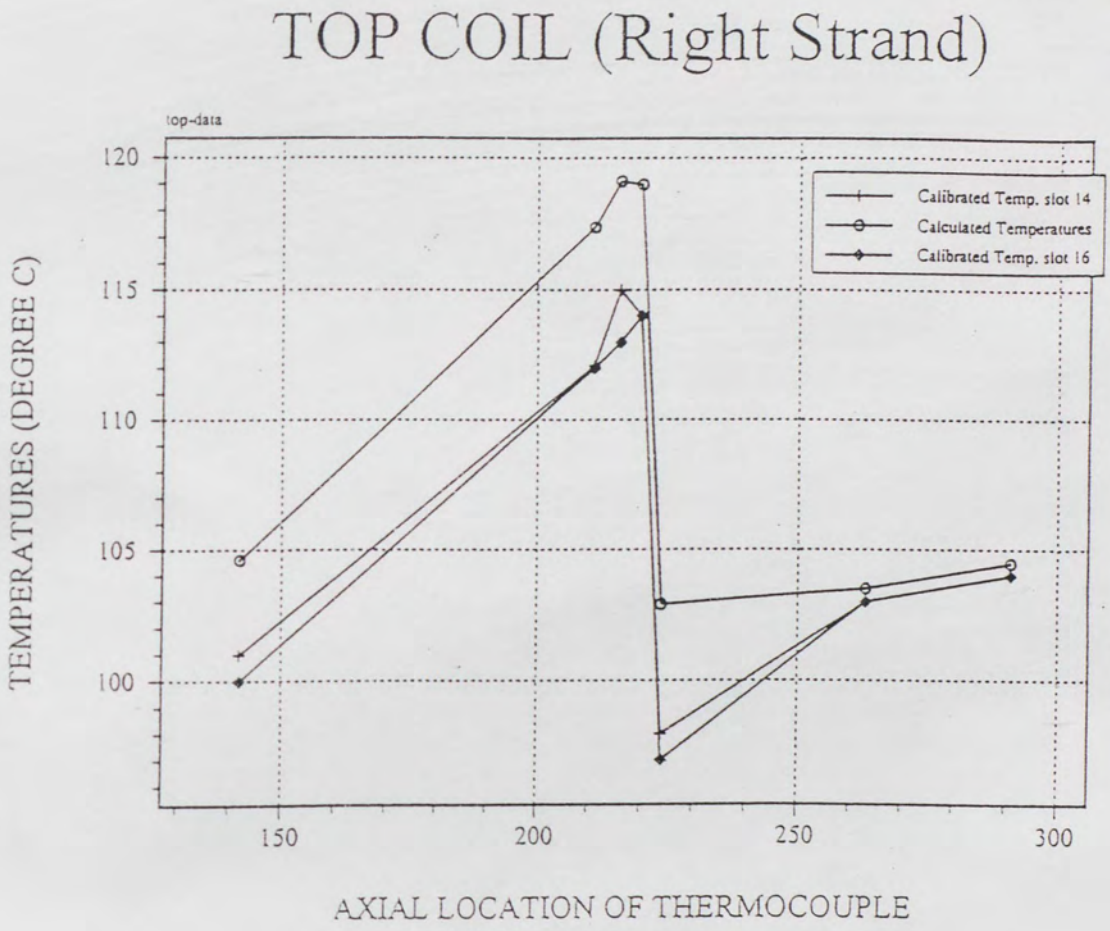

FIGURE 27. Top Coil Right Strand Temperature Profile

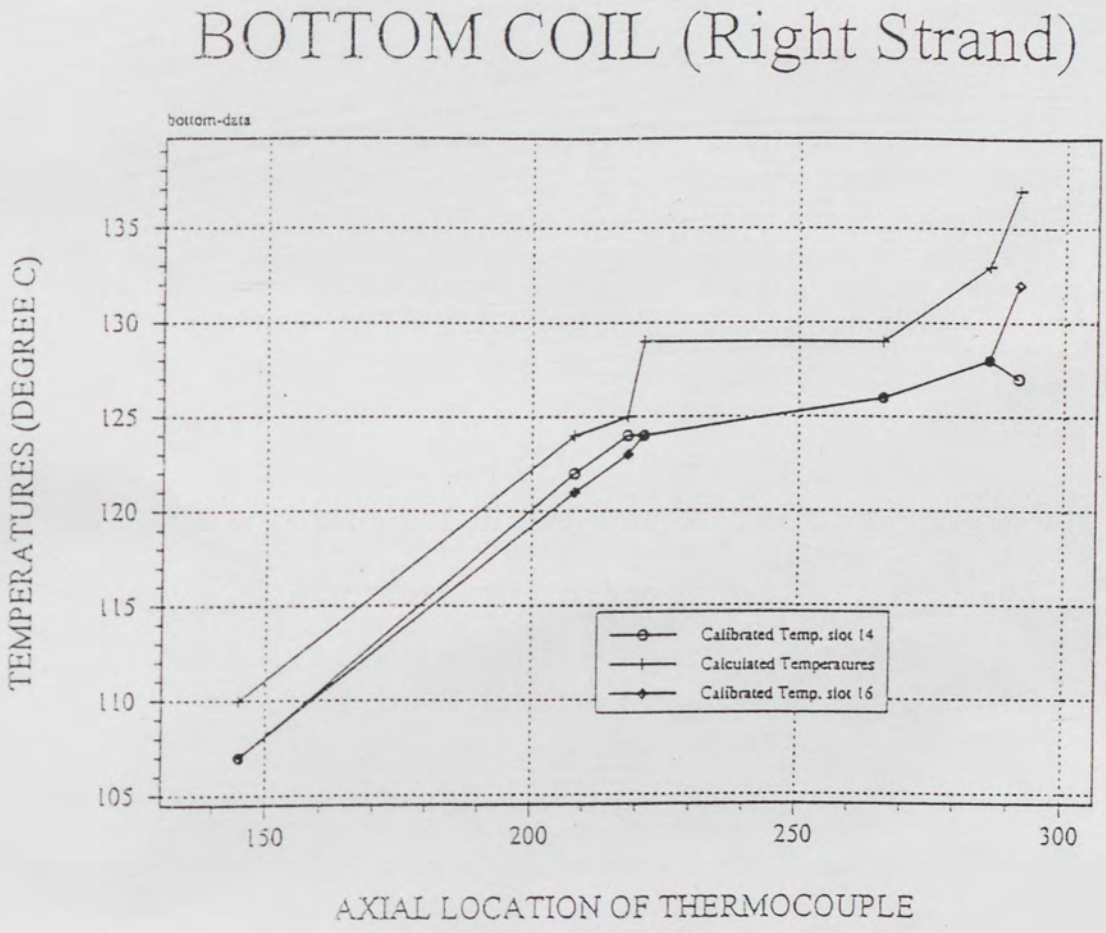

FIGURE 28. Bottom Coil Right Strand Temperature Profile

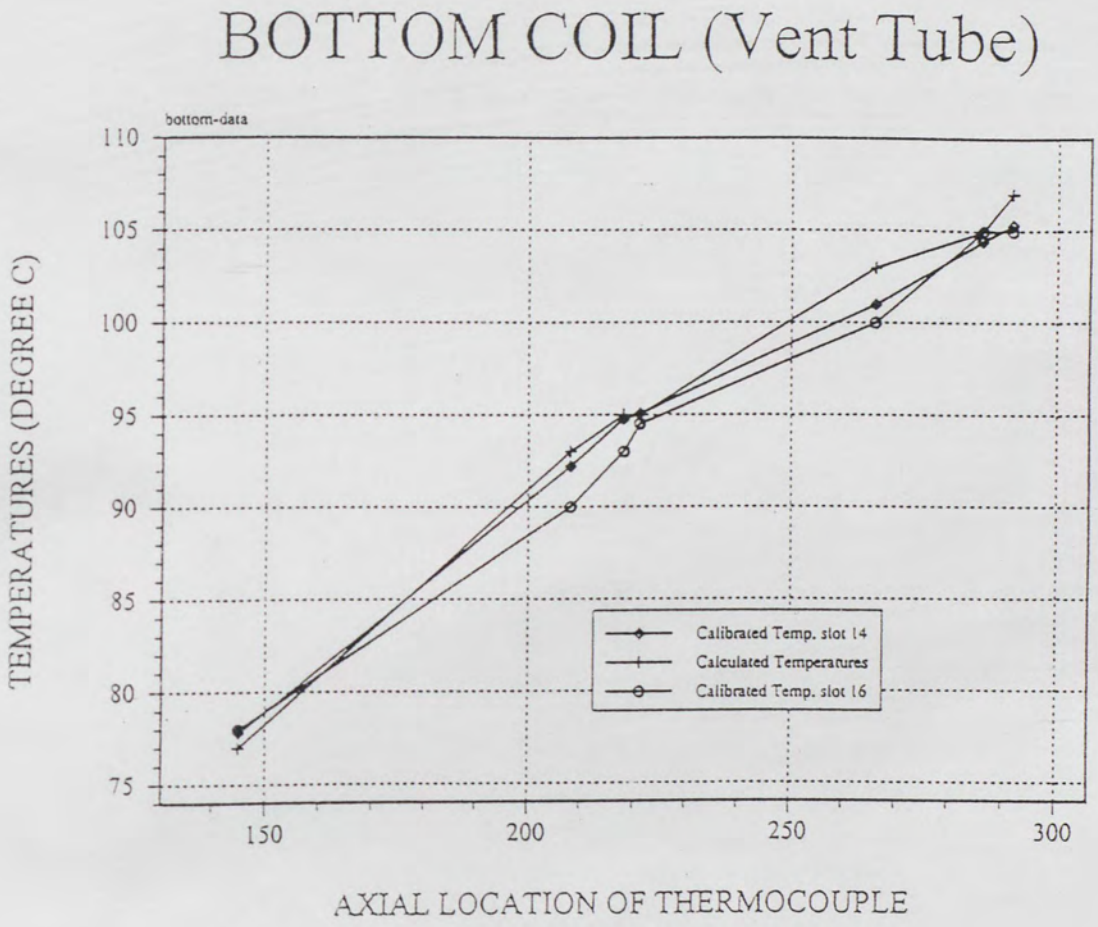

FIGURE 29. Bottom Coil Vent Tube Temperature Profile

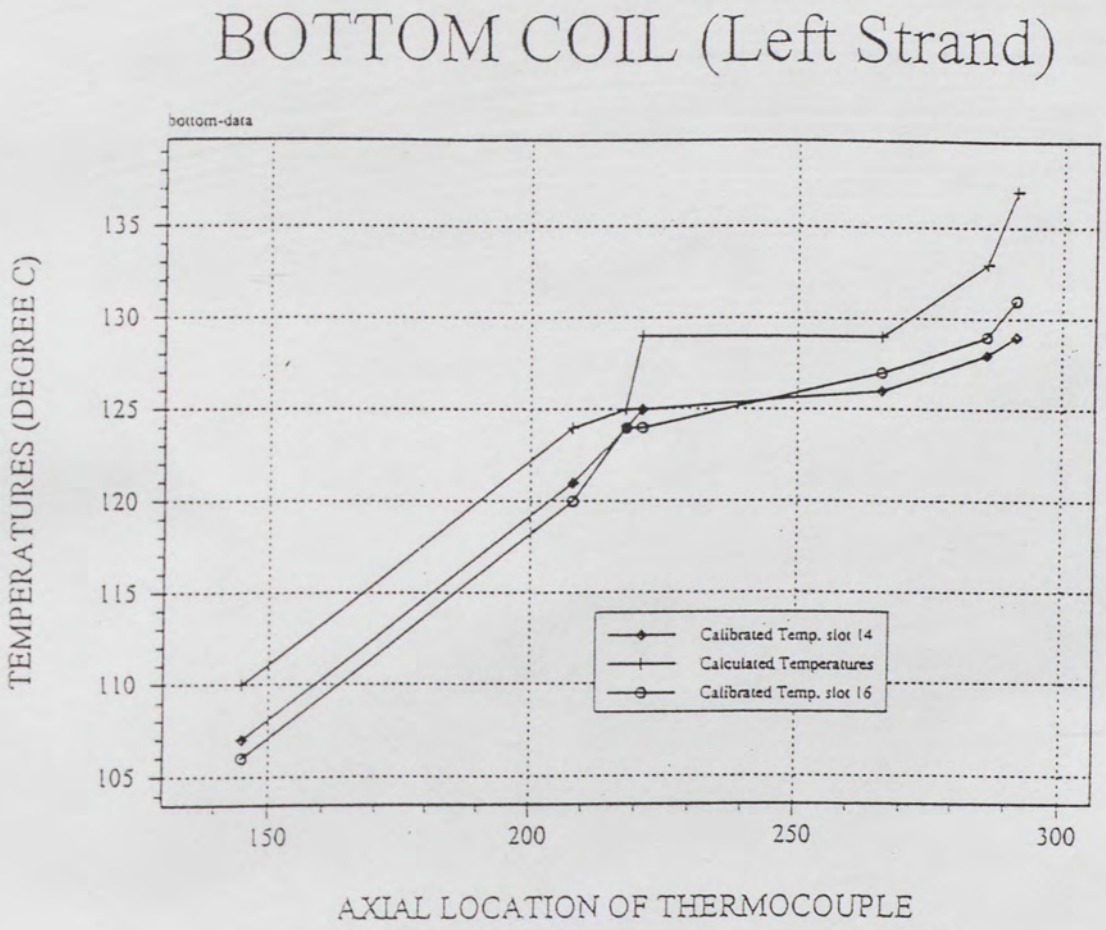

FIGURE 30. Bottom Coil Left Strand Temperature Profile

AXIAL LOCATION	SHORT CIRCUITED DATA	OPEN CIRCUITED DATA	CALIBRATED FULL LOAD DATA
142 inches			
left strand	97°C	50°C	101°C
vent tube	70.4	46.6	71
right strand	95.9	50.1	100
211 inches			
left strand	105.1	53.9	113
vent tube	77.4	50.6	82
right strand	107.25	50.75	112
216 inches			
left strand	103.75	56.25	114
vent tube	80.25	49.25	83.5
right strand	103.8	55.2	113
220 inches			
left strand	111	50	115
vent tube	83.5	46.9	84.4
right strand	110	50	114
224 inches			
left strand	95	48	99
vent tube	78.65	49.35	82
right strand	92.95	50.05	97
263 inches			
left strand	100.95	49.05	104
vent tube	81.7	49.3	85
right strand	99	50	103
291 inches			
left strand	98	51	103
vent tube	84.5	49.5	88
right strand	99.5	50.5	104

TABLE 1. Top Coil Test Values (Slot 16)

AXIAL LOCATION	SHORT CIRCUITED DATA	OPEN CIRCUITED DATA	CALIBRATED FULL LOAD DATA
145 inches			
left strand	102°C	50°C	106°C
vent tube	77.3	46.7	78
right strand	103	50.	107
208 inches			
left strand	112.1	53.9	120
vent tube	85.4	50.6	90
right strand	116.25	50.75	121
218 inches			
left strand	113.75	56.25	124
vent tube	89.75	49.25	93
right strand	115.8	55.2	123
221 inches			
left strand	120	50	124
vent tube	93.6	46.9	94.5
right strand	120.1	49.9	124
266 inches			
left strand	125	48	127
vent tube	96.65	49.35	100
right strand	121.95	50.05	126
286 inches			
left strand	125.95	49.05	129
vent tube	101.7	49.3	105
right strand	124	50	128
291.5 inches			
left strand	126	51	131
vent tube	101.4	49.6	105
right strand	127.9	50.1	132

TABLE 2. Bottom Coil Test Values (Slot 16)

OLD METHOD		BOTTOM COIL		SLOT 16		
		°C				
Axial location from Exciter End (inches)	*Short Circuit Test Data*	*Open Circuit Test Data*	*Calibrated Loaded Test Data*	*Calculated Loaded Data*	*Calculated minus Calibrated*	
142" (center of core)						
Left Strand	97	50	101	123	22	
Vent Tube	70.4	46.6	71	81	10	
Right Strand	95.9	50.1	100	123	23	
220" (end of core)						
Left Strand	111	50	115	130	15	
Vent Tube	83.5	46.9	84.4	88	3.6	
Right Strand	110	50	114	130	16	
291" (end of coil)						
Left Strand	98	51	103	122	19	
Vent Tube	84.5	49.5	88	95	7	
Right Strand	99.5	50.5	104	122	18	

TABLE 3. Test Data compared to Calculated Data
(Calculated data completed by traditional methods {old methods})

		TOP COIL		SLOT 14		
		°C				
Axial location from Exciter End (inches)	*Short Circuit Test Data*	*Open Circuit Test Data*		*Calibrated Loaded Test Data*	*Calculated Loaded Data*	*Calculated minus Calibrated*
142" (center of core)						
Left Strand	96.1	49.9		100	104.62	4.62
Vent Tube	69.22	46.85		70.07	72	1.93
Right Strand	97.3	49.7		101	104.62	3.62
220" (end of core)						
Left Strand	110.6	50.1		114.7	119	4.3
Vent Tube	83.52	47.1		84.62	85	0.38
Right Strand	110.1	49.9		114	119	5
291" (end of coil)						
Left Strand	97.89	51.2		103.09	104.48	1.39
Vent Tube	84.15	49.2		87.35	89	1.65
Right Strand	99.3	50.7		104	104.48	0.48

TABLE 4. Test Data compared to Calculation Data
(Calculation data completed by improved methods described in this thesis)

		TOP COIL °C		SLOT 16		
Axial location from Exciter End (inches)	*Short Circuit Test Data*	*Open Circuit Test Data*		*Calibrated Loaded Test Data*	*Calculated Loaded Data*	*Calculated minus Calibrated*
142" (center of core)						
Left Strand	97	50		101	104.62	3.62
Vent Tube	70.4	46.6		71	72	1
Right Strand	95.9	50.1		100	104.62	4.62
220" (end of core)						
Left Strand	111	50		115	119	4
Vent Tube	83.5	46.9		84.4	85	0.6
Right Strand	110	50		114	119	5
291" (end of coil)						
Left Strand	98	51		103	104.48	1.48
Vent Tube	84.5	49.5		88	89	1
Right Strand	99.5	50.5		104	104.48	0.48

TABLE 5. Test Data compared to Calculation Data
(Calculation data completed by improved methods described in this thesis)

		BOTTOM COIL °C		SLOT 14		
Axial location from Exciter End (inches)	*Short Circuit Test Data*	*Open Circuit Test Data*		*Calibrated Loaded Test Data*	*Calculated Loaded Data*	*Calculated minus Calibrated*
145" (center of core)						
Left Strand	103.2	49.8		107	110	3
Vent Tube	77	46.8		77.8	77	-0.8
Right Strand	103.3	49.7		107	110	3
221" (end of core)						
Left Strand	121	50		125	129	4
Vent Tube	94.06	47		95.06	95	-0.06
Right Strand	120.1	49.9		124	129	5
291.5" (end of coil)						
Left Strand	123.9	51.1		129	137	8
Vent Tube	102.15	49.2		105.35	107	1.65
Right Strand	122.3	50.7		127	137	10

TABLE 6. Test Data compared to Calculation Data
(Calculation data completed by improved methods described in this thesis)

		BOTTOM COIL °C	SLOT 16		
Axial location from Exciter End (inches)	*Short Circuit Test Data*	*Open Circuit Test Data*	*Calibrated Loaded Test Data*	*Calculated Loaded Data*	*Calculated minus Calibrated*
145" (center of core)					
Left Strand	102	50	106	110	4
Vent Tube	77.3	46.7	78	77	-1
Right Strand	103	50	107	110	3
221" (end of core)					
Left Strand	120	50	124	129	5
Vent Tube	93.6	46.9	94.5	95	0.5
Right Strand	120.1	49.9	124	129	5
291.5" (end of coil)					
Left Strand	126	51	131	137	6
Vent Tube	101.4	49.6	105	107	2
Right Strand	127.9	50.1	132	137	5

TABLE 7. Test Data compared to Calculation Data
(Calculation data completed by improved methods described in this thesis)

CONCLUSION

As the power industry strive to increase overall plant efficiencies, there tends to be a growing demand for more efficient electric generators. A major limiting factor in determining the maximum rating of an electric generator is the hot spot temperatures located in the stator coils. To try and meet the demand for more efficient electric generators, new stator coil designs are being manufactured.

Using the present method of calculating hot spot temperatures on the recently designed test machine refereed to in this thesis showed a difference in calculated vs tested temperatures of 7 to 23°C. This large temperature difference requires that the machine be derated to ensure that it operates properly throughout its design life; therefore, the machine is not being used to its full potential and therefore is not as efficient as it could be.

The purpose of this thesis was to develop a more accurate method of calculating hot spot temperatures by more accurately calculating the cross slot flux and its associated losses. Unlike past calculations which used average cross flux in all cross slot flux loss calculations, this thesis developed the individual cross slot flux for each strand in the roebel bar therefore more accurately calculating its associated losses and circulating currents. The results of using the improved method developed in this thesis were very

positive. The temperature difference between tested and calculated values were between 2 to 10°C. This is a substantial improvement (two hundred percent better) from the results using the present (traditional) calculation methods.

Although very positive, this calculation method was verified with only one type of roebel transposition (720° roebel) and was tested on only one machine. The improved method described in the paper can be applied to various roebel transpositions with solid end connections; but more tests should follow to identify all the practical applications for these improved cross slot flux loss calculations. The effects of radial flux were assumed negligible for this application because of the distance of the top coil below the stator bore. However, radial flux and its effects on the cross slot flux should be investigated for larger machines where the radial flux becomes very significant. Also, machines without series connections, such as water cooled coils, have significant roebel to roebel bar circulating currents and provisions to more accurately calculate these losses should be considered.

REFERENCES

[1]. American National Standard for Rotating Electrical Machinery, "Cylindrical-Rotor Synchronous Generators", ANSI C50.13-1989

[2]. G. Neidhoefer, "Roebel Bar Windings for Large Synchronous Machines", BBC Review Vol. 57, January 1970

[3]. A.E. Fitzgerald, Charles Kingsley Jr., Stephen D. Umans, Electric Machinery, McGraw-Hill, New York, NY, 1983

[4]. American National Standard, "General Requirements for Synchronous Machines", ANSI C50.10-1977

[5]. B.J. Bennington, "Eddy Currents in a Transposed Turbo-Generator Coil Side, Short Circuited at Each End", Westinghouse Internal Technical Report 371, 1967

[6]. William H. Timbie, Vannevar Bush, Principles of Electrical Engineering, John Wiley & Sons, 1947

[7]. W.L. Ringland, L.T. Rosenberg, "A New Stator Coil for Large Machines", AIEE Transactions (Power Apparatus and Systems), Vol 78, Oct. 1959

[8]. R.E. Gilman, "Eddy Current Losses in Armature Conductors", AIEE Transactions (Power Apparatus and Systems); Vol. 39, 1920; continued in Vol 43, 1924

[9]. B.J. Bennington, W.C. Brenner, "Transpositions in Turbogenerator Coil Sides Short Circuited at Each End", IEEE PAS Vol PAS-89, #8, Nov/Dec 1970

[10]. M. Matsusaki, "Theory of Eddy Current Calculation in a Turbo-Generator Stator Coil Side Short-Circuited at Each End", Westinghouse Internal Technical Report 87025, 1987

[11]. E.I. King, "Equivalent Circuits for Two-Dimensional Magnetic Fields", IEEE PAS Vol PAS-85, #9, Sept 1966

[12]. M. Matsusaki, "Current Distribution in a Turbo-Generator Stator Coil Side with Various Transpositions", Westinghouse Internal Technical Report 87095, 1987

[13]. A. Prole, "The Influence of Deep Bar Losses in Design of Stator Coils", Westinghouse Internal Technical Paper, 1988

[14]. M. Iseli, K. Reichert, G. Neidhofer, "Calculation of Current Distribution and Stray Losses in Arbitrarily Transposed Stator Coils", International Conference on Electric Machines, Pisa, Italy, Proceedings Vol II, 1988.

[15]. K.M. Sochats, "Waterwheel RTD Temperature Prediction Program", Westinghouse Internal Technical Report 489, 1971.

[16]. Institute of Electrical and Electronics Engineers, "Test Procedures for Synchronous Machines", IEEE Std 115-1983.